Task-Related Component Analysis for Functional Neuroimaging and Application to Near-Infrared Spectroscopy Data

Hirokazu Tanaka[a*, **], *Takusige Katura*[b*, **], *and Hiroki Sato*[b]

a. School of Information Science
Japan Advanced Institute of Science and Technology
1-1 Asahidai, Nomi, Ishikawa 923-1211, Japan

b. Central Research Laboratory, Hitachi, Ltd.
2520 Akanuma, Hatoyama, Saitama 350-0395, Japan

* Equally contributed
** Corresponding authors

Text page: 46
Figures: 12
Abstract: 264 words
Introduction: 670 words

Abbreviated Title: Task-Related Component Analysis

Corresponding authors:
Hirokazu Tanaka
Email: hirokazu@jaist.ac.jp
Tel: +81-761-51-1226 Fax: +81-761-51-1149
Takusige Katura
Email: takusige.katura.ny@hitachi.com
Tel: +81-49-296-6111 Fax: +81-49-296-5999

Key words: Correlation Maximization; Covariance Maximization; Functional Neuroimaging; Optical Topography; Biomedical Data Analysis; Rayleigh-Ritz Problem

ABSTRACT

Reproducibility of experimental results lies at the heart of scientific disciplines. Here we propose a signal processing method that extracts task-related components by maximizing the reproducibility during task periods from neuroimaging data. Unlike hypothesis-driven methods such as general linear models, no specific time courses are presumed, and unlike data-driven approaches such as independent component analysis, no arbitrary interpretation of components is needed. Task-related components are constructed by a linear, weighted sum of multiple time courses, and its weights are optimized so as to maximize inter-block correlations (CorrMax) or covariances (CovMax). Our analysis method is referred to as task-related component analysis (TRCA). The covariance maximization is formulated as a Rayleigh-Ritz eigenvalue problem, and corresponding eigenvectors give candidates of task-related components. In addition, a systematic statistical test based on eigenvalues is proposed, so task-related and -unrelated components are classified objectively and automatically. The proposed test of statistical significance is found to be independent of the degree of autocorrelation in data if the task duration is sufficiently longer than the temporal scale of autocorrelation, so TRCA can be applied to data with autocorrelation without any modification. We demonstrate that simple extensions of TRCA can provide most distinctive signals for two tasks and can integrate multiple modalities of information to remove task-unrelated artifacts. TRCA was successfully applied to synthetic data as well as near-infrared spectroscopy (NIRS) data of finger tapping. There were two statistically significant task-related components; one was a hemodynamic response, and another was a piece-wise linear time course. In summary, we conclude that TRCA has a wide range of applications in multi-channel biophysical and behavioral measurements.

1. INTRODUCTION

Analysis of neuroimaging data can be in general classified into two categories: a hypothesis-driven approach such as general linear models (GLMs), and a data-driven approach such as principle component analysis (PCA) and independent component analysis (ICA). Hypothesis- and data-driven approaches correspond to supervised and unsupervised approaches, respectively, in machine learning. In the hypothesis-driven approach, a single time course obtained in neuroimaging data is assumed to consist of certain specific task-related components (e.g., hemodynamic responses) and task-unrelated components (e.g., systemic signals and head movement artifacts). In GLMs, these presumed components are summarized in a so-called design matrix, and their contributions are statistically assessed by the statistical parametric mapping (SPM) method (Friston et al., 1994b). For analysis of functional magnetic resonance imaging (fMRI) data, GLM and SPM have been highly successful in localizing voxels that show significant activations related to a task. The GLM analysis, however, requires certain hypotheses about task-related and task-unrelated components, which may not be a priori obvious in some cases such as the shape of hemodynamic response function (Plichta et al., 2007). Furthermore, GLM is not able to assess components that are not modeled into a design matrix.

Another approach to neuroimaging data analysis is the data-driven approach in which only general statistical assumptions are made to decompose neuroimaging data. One notable example is ICA, in which only statistical independence between source signals is assumed (Bell and Sejnowski, 1995; Amari et al., 1996; Hyvarinen and Oja, 1997). ICA extracts independent components as a linear weighted sum of multiple time series and maximizes some information-theoretic criteria such as mutual information or higher-order cumulants. ICA has been successfully applied to fMRI, electroencephalography (EEG) and near-infrared spectroscopy (NIRS) data analyses (Makeig et al., 1996; McKeown and Sejnowski, 1998; Kohno et al., 2007; Katura et al., 2008). In contrast to GLM,

ICA makes no assumptions other than statistical independence between source signals, so it can sometimes discover unexpected components in neuroimaging data. Moreover, its applicability is not limited to neuroimaging data but also covers physiological and behavioral data (Nakamura et al., 2004). Independent components discovered by ICA, however, need an additional process for determining which of independent components are task-related or artifactual (Nakada et al., 2000). Also, due to its generality, the original formulation of ICA does not make any use of available information regarding experimental procedures (there are a few extensions of ICA that incorporate temporal or spatial constraints, though (Calhoun et al., 2005; Lin et al., 2010)).

We here propose a new analysis approach to extract task-related components from a linear weighted sum of multiple time series. This analysis will be referred to as *task-related component analysis* (TRCA). Coefficients, or weights, of time series are determined so as to maximize the covariance or correlation between task blocks, thereby maximizing the inter-block consistency. This is based on a belief that a signal that appears consistently and robustly in every task block should be regarded as task related. In other words, we define task relatedness by consistent and robust appearance of a same signal. This covariance-maximization problem is formulated as a Rayleigh-Ritz eigenvalue problem, and statistical significance of each solution can be assessed by a corresponding eigenvalue. Unlike GLM, TRCA assumes no a priori knowledge of time series other than task periods, and unlike ICA, TRCA can provide a concrete measure of task-relatedness to each extracted component. In GLM analyses, autocorrelation in time series poses a serious issue of inflated statistics, but we show that TRCA is not sensitive to autocorrelation if the time scale of temporal smoothing is smaller than the duration of task block. Furthermore, we show that TRCA can be generalized into a classification problem of binary tasks and can sequentially incorporate known effects obtained from an additional source such as respiration and body motion in order to remove task-unrelated artifacts. We illustrate our proposed method by applying to synthetic data and NIRS

data. Although our method has been developed mainly for NIRS data analysis, we argue that it has a wide applicability to multi-channel physiological and behavioral measurements.

2. METHODS

Section 2.1 illustrates a linear generative model of observed time courses and explains the concept that covariance maximization can recover task-related components. Section 2.2 formulates TRCA by using two conventional measures; a correlation coefficient and covariance, and Section 2.3 proposes a statistical test for choosing significantly task-related components. Section 2.4 argues how autocorrelation due to temporal smoothing affects results of the statistical test. Sections 2.5 and 2.6 explain simple extensions of our method for multiple tasks and for data augmentation, respectively. These extensions are not easily realized with PCA or ICA. Section 2.7 argues how to obtain a spatial map of task-related component. Finally, Sections 2.8 and 2.9 summarize details of synthetic and NIRS data. Further tests of the methods are described in Supplementary Material.

2.1. Signal Reconstruction from Weighted Linear Summation

We here illustrate the concept of task-related component analysis by a simple example. Two signal sources are assumed when there are three blocks of a task; one ($s(t)$: task related) that has the same profile during every task block (i.e., $s^{(1)}(t)$, $s^{(2)}(t)$ and $s^{(3)}(t)$ are the same, sustained wave forms) (Figure 1A, top), and another ($n(t)$: task unrelated) that is flat except the second block (i.e., $n^{(2)}(t)$ is phasic whereas $n^{(1)}(t)$ and $n^{(3)}(t)$ are flat) (Figure 1A, bottom). These signal time courses are constructed so that covariance between blocks of the task-related component is a positive constant ($\mathrm{Cov}\left(s^{(1)}(t), s^{(2)}(t)\right) = \mathrm{Cov}\left(s^{(1)}(t), s^{(3)}(t)\right) = \mathrm{Cov}\left(s^{(2)}(t), s^{(3)}(t)\right) = \text{positive const}$) whereas covariance between blocks of the task-unrelated component and between task-related and

task-unrelated are zero ($\mathrm{Cov}\left(s^{(i)}(t), n^{(j)}(t)\right) = \mathrm{Cov}\left(n^{(i)}(t), n^{(j)}(t)\right) = 0 \ \left(1 \le i < j \le 3\right)$). A linear generative model of observed time courses ($x_1(t)$ and $x_2(t)$) are assumed as

$$\begin{cases} x_1(t) = a_{11}s(t) + a_{12}n(t) \\ x_2(t) = a_{21}s(t) + a_{22}n(t) \end{cases}, \tag{1}$$

as illustrated in Figure 1B. The problem is to recover the latent task related component $s(t)$ from a linear sum of observed time courses defined as

$$y(t) = w_1x_1(t) + w_2x_2(t) = \left(w_1a_{11} + w_2a_{21}\right)s(t) + \left(w_1a_{12} + w_2a_{22}\right)n(t). \tag{2}$$

We propose to maximize the covariance of the first-block ($y^{(1)}(t)$) and the second-block ($y^{(2)}(t)$) time course (here, for simplicity, covariance between first and second blocks is considered, and a multiple-block case will be discussed in the following subsection):

$$\begin{aligned} \mathrm{Cov}\left(y^{(1)}, y^{(2)}\right) &= \left(w_1a_{11} + w_2a_{21}\right)^2 \mathrm{Cov}\left(s^{(1)}, s^{(2)}\right) + \left(w_1a_{12} + w_2a_{22}\right)^2 \mathrm{Cov}\left(n^{(1)}, n^{(2)}\right) \\ &\quad + \left(w_1a_{11} + w_2a_{21}\right)\left(w_1a_{12} + w_2a_{22}\right)\left[\mathrm{Cov}\left(s^{(1)}, n^{(2)}\right) + \mathrm{Cov}\left(n^{(1)}, s^{(2)}\right)\right]. \\ &= \left(w_1a_{11} + w_2a_{21}\right)^2 \mathrm{Cov}\left(s^{(1)}, s^{(2)}\right) \end{aligned} \tag{3}$$

Here we used $\mathrm{Cov}\left(n^{(1)}, n^{(2)}\right) = \mathrm{Cov}\left(s^{(1)}, n^{(2)}\right) = \mathrm{Cov}\left(n^{(1)}, s^{(2)}\right) = 0$. This is a quadratic function of w_1 and $w_{2,}$ which is unbounded. To obtain a finite solution, the variance of $y(t)$ is constrained to be one,

$$\mathrm{var}\left(y\right) = \left(w_1a_{11} + w_2a_{21}\right)^2 + \left(w_1a_{12} + w_2a_{22}\right)^2 = 1, \tag{4}$$

where the signals are assumed to be normalized ($\mathrm{Var}\left(s(t)\right)=\mathrm{Var}\left(n(t)\right)=1$) and uncorrelated ($\mathrm{Cov}\left(s(t),n(t)\right)=0$). This constrained optimization problem has a solution of $w_1a_{11}+w_2a_{21}=1$ and $w_1a_{12}+w_2a_{22}=0$, leading to the final solution $y(t)=s(t)$ unless $a_{11}a_{22}-a_{12}a_{21}=0$. This simple example suggests that inter-block covariance maximization can be a guiding principle for reconstructing task-related components from observed time courses. The following sections will discuss general multiple time-course cases.

2.2. Task-Related Component Analysis: A Basic Formulation

Suppose that *N*-channel temporal signals denoted by $x_i(t)$ (i=1,…,N) are given, containing K blocks of a same repeated task whose periods are fixed as $t\in[t_k,t_k+T]$ $(k=1,\cdots,K)$. Here T is duration of each task block. We propose that a task-related component is computed as a linear, weighted sum of those input signals as:

$$y(t)=\sum_{i=1}^{N}w_ix_i(t)=\mathbf{w}^{\mathrm{T}}\mathbf{x}(t). \tag{5}$$

As in the previous section, we implicitly assume that observed signals are generated by a linear weighted sum of task-related and task-unrelated components so that task-related components can be recovered by appropriately weighing observed signals. The goal of this analysis is to optimize the coefficients in such a way that a temporal profile of task-related component exhibits a maximal temporal similarity among task blocks, as illustrated in Figure 1C. We will formulate this problem in two distinct but related ways; Correlation maximization and covariance maximization.

Correlation Maximization (CorrMax)

One such a measure of reproducibility is a correlation coefficient between *k*- and *l*-th blocks

defined by

$$C_{kl} = \mathrm{Corr}\left(y^{(k)}(t), y^{(l)}(t)\right) = \frac{\sum_{i,j} w_i w_j \mathrm{Cov}\left(x_i^{(k)}(t), x_j^{(l)}(t)\right)}{\sqrt{\sum_{i,j} w_i w_j \mathrm{Cov}\left(x_i^{(k)}(t), x_j^{(k)}(t)\right)} \sqrt{\sum_{i,j} w_i w_j \mathrm{Cov}\left(x_i^{(l)}(t), x_j^{(l)}(t)\right)}}. \quad (6)$$

Here $y^{(k)}(t)$ and $x_i^{(k)}(t)$ denote a *k*-th block segment of $y(t)$ and $x_i(t)$, respectively. We propose to maximize the sum of correlation coefficients between all possible combinations of task blocks defined as

$$\sum_{\substack{k,l=1 \\ k \neq l}}^{K} C_{kl} = \sum_{\substack{k,l=1 \\ k \neq l}}^{K} \mathrm{Corr}\left(y^{(k)}(t), y^{(l)}(t)\right) = \sum_{\substack{k,l=1 \\ k \neq l}}^{K} \frac{\sum_{i,j} w_i w_j \mathrm{Corr}\left(x_i^{(k)}(t), x_j^{(l)}(t)\right)}{\sqrt{\sum_{i,j} w_i w_j \mathrm{Corr}\left(x_i^{(k)}(t), x_j^{(k)}(t)\right)} \sqrt{\sum_{i,j} w_i w_j \mathrm{Corr}\left(x_i^{(l)}(t), x_j^{(l)}(t)\right)}}. \quad (7)$$

This objective function is invariant to a global rescaling of weight coefficients $w_i \to \alpha w_i$, so in order to bound the coefficients, the variance of *y*(*t*) is normalized to one as

$$\mathrm{Var}\left(y(t)\right) = \sum_{i,j=1}^{N} w_i w_j \mathrm{Cov}\left(x_i(t), x_j(t)\right) = \mathbf{w}^{\mathrm{T}} \mathbf{Q} \mathbf{w} = 1, \quad (8)$$

where $(\mathbf{Q})_{ij} \equiv \mathrm{Cov}\left(x_i(t), x_j(t)\right)$. This formulation is referred to as correlation maximization (CorrMax). The objective function (Eq. (7)) is nonlinear in terms of the weight coefficients due to the quadratic terms in the denominators, so an analytical, closed-form solution cannot be expected. Instead, a numerical optimization algorithm (fmincon of MATLAB Optimization Toolbox, MathWorks, MA, U.S.A.) was used.

Covariance Maximization (CovMax)

Although it is reasonable to maximize the sum of inter-block correlations (Eq. (7)), the computation for optimization does not have an analytically closed form, and more seriously, only a single task-related component is obtained. Instead of correlation coefficients, we propose an alternative way to maximize covariance between *k*-th and *l*-th blocks of $y(t)$:

$$\hat{C}_{kl} = \mathrm{Cov}\left(y^{(k)}(t), y^{(l)}(t) \right) = \sum_{i,j=1}^{N} w_i w_j \mathrm{Cov}\left(x_i^{(k)}(t), x_k^{(l)}(t) \right). \tag{9}$$

As in Eq. (7), all possible combinations of task blocks are summed as

$$\begin{aligned} \sum_{\substack{k,l=1 \\ k \neq l}}^{K} \hat{C}_{kl} &= \sum_{\substack{k,l=1 \\ k \neq l}}^{K} \mathrm{Cov}\left(y^{(k)}(t), y^{(l)}(t) \right) \\ &= \sum_{\substack{k,l=1 \\ k \neq l}}^{K} \sum_{i,j=1}^{N} w_i w_j \mathrm{Cov}\left(x_i^{(k)}(t), x_j^{(l)}(t) \right) = \mathbf{w}^{\mathrm{T}} \mathbf{S} \mathbf{w} \end{aligned}. \tag{10}$$

Here the symmetric matrix **S** is defined by

$$\left(\mathbf{S} \right)_{ij} \equiv \sum_{\substack{k,l=1 \\ k \neq l}}^{K} \mathrm{Cov}\left(x_i^{(k)}(t), x_j^{(l)}(t) \right). \tag{11}$$

We propose to maximize the quantity defined in Eq. (10), which will be referred to as *task consistency*. This formulation is referred to as covariance maximization (CovMax). Note that inputs required by TRCA are only task block timings. As in the CorrMax algorithm, the normalization constraint (Eq. (8)) is imposed. Now the constrained optimization problem becomes a Rayleigh-Ritz

eigenvalue problem:

$$\hat{\mathbf{w}} = \arg\max_{\mathbf{w}} \frac{\mathbf{w}^{\mathrm{T}}\mathbf{S}\mathbf{w}}{\mathbf{w}^{\mathrm{T}}\mathbf{Q}\mathbf{w}}. \tag{12}$$

With the help of the Rayleigh-Ritz theorem, the optimal coefficient vector is obtained as an eigenvector of the matrix $\mathbf{Q}^{-1}\mathbf{S}$. A Matlab function to solve this eigenvalue problem was included in Appendix A. Generally N eigenvectors of the matrix $\mathbf{Q}^{-1}\mathbf{S}$ are obtained, and correspondingly N components are obtained. Without loss of generality, task-related components are arranged in a descending order of associated eigenvalues. These eigenvalues can be used to statistically test whether the corresponding components are task-related or not, as discussed in the next subsection. Throughout this paper, the CovMax algorithm will be used otherwise stated.

2.3. Statistical Test of Task Consistency

In order to assess how significantly task-related the components are, a statistical test must be introduced. One such measure is an eigenvalue λ of the matrix $\mathbf{Q}^{-1}\mathbf{S}$, which represents the value of cost function for the corresponding eigenvector $\hat{\mathbf{w}}$:

$$\hat{\mathbf{w}}^{T}\mathbf{S}\hat{\mathbf{w}} = \frac{\hat{\mathbf{w}}^{T}\mathbf{S}\hat{\mathbf{w}}}{\hat{\mathbf{w}}^{T}\mathbf{Q}\hat{\mathbf{w}}} = \frac{\lambda\hat{\mathbf{w}}^{T}\mathbf{Q}\hat{\mathbf{w}}}{\hat{\mathbf{w}}^{T}\mathbf{Q}\hat{\mathbf{w}}} = \lambda \quad \left(\because \mathbf{S}\hat{\mathbf{w}} = \lambda\mathbf{Q}\hat{\mathbf{w}}\right). \tag{13}$$

Therefore, the eigenvalue represents the task consistency among task blocks. If the original signals contain no task related components but just random variations, corresponding eigenvalues will be limited to a chance range.

Mathematics of random matrices has been well investigated from the seminal work of Wigner, who explained the energy spectrum of an atomic nucleus as an eigenvalue distribution of a random matrix (Wigner, 1955, 1967). When x_i's are temporally uncorrelated random variables, the matrix **Q** in Eq. (8) is known as the Wishart matrix (Wishart, 1928) and its eigenvalue distribution is known in the limit of infinite *N* and *T* known as Marcenko-Pastur's quarter circle law (Marcenko and Pastur, 1967). This formula has been used to assess statistical significance of principal components of spike ensemble recording (Peyrache et al., 2010). The analytical formula assumes no temporal correlation between input time courses $\{x_i\}$, whereas there are considerable temporal autocorrelations in biological signals. Therefore, a statistical test based on the analytical formula is not appropriate for our case.

We here take a more practical and computational approach, in which the weight distribution when a null hypothesis is assumed is to use a non-parametric, permutation test. Our null hypothesis postulates that there is no task related component; therefore, instead of actual task onsets $\{t_k\}$ $(k = 1, \cdots, K)$, randomized task-block onsets (*K* time points sampled from a uniform distribution of entire experimental duration) can be used to compute the null distribution of weight coefficients. This gives the null distribution of weight coefficients, so a statistical significance of actual coefficients can be quantified by comparing with the null distribution. Eigenvalues outside a confidence interval of the null distribution can be regarded as being statistically significant, and corresponding eigenvectors can be regarded as being task related.

To summarize, TRCA consists of three computational steps: (1) computation of eigenvalues and eigenvectors of the matrix $\mathbf{Q}^{-1}\mathbf{S}$ with experimentally given periods of task blocks, (2) computation of the weight distribution with randomized periods of task blocks, and (3) selection of statistically significant task-related components. The procedure for computing task related components is schematically summarized in Figure 2.

2.4. Effect of Temporal Smoothing and Autocorrelation

Neuroimaging data such as BOLD signals in fMRI and oxy- and dexoy-hemoglobin concentration signals in NIRS contain considerable temporal autocorrelation due to inherent slow hemodynamic responses. Autocorrelation in the signals is enhanced by temporal smoothing, which is often employed for the purpose of artifact removal and the improvement of signal detection. In standard GLM methods, such autocorrelation leads to underestimation of the noise variance and hence to the inflation of estimated statistics (e.g., the *t*-statistic, which is inversely proportional to the noise variance). Considerable efforts have been made to develop methods to evaluate the degree of autocorrelation in data and to correct the statistic both in fMRI (Friston et al., 1994a; Friston et al., 1995; Worsley and Friston, 1995; Friston et al., 2000) and in NIRS (Fekete et al., 2011).

It is thus important to assess whether and how inflated autocorrelation due to inherent hemodynamics and temporal smoothing affects the results of the statistical analysis of TRCA because temporal smoothing induces spurious correlation and covariance. At first one might think that an appropriate correction is required when the method is applied to input time courses with considerable temporal autocorrelation because autocorrelation generally increases our covariance measure (Eq. (10)). However, as seen in Eq. (13), the optimal coefficient is determined as a tradeoff between the inter-block covariance (Eq. (10)) and the covariance of entire time courses (Eq. (8)), the latter of which also increases with temporal smoothing. The statistical test of TRCA uses the eigenvalues of the matrix $\mathbf{Q}^{-1}\mathbf{S}$ but not the individual matrices $\mathbf{Q}$ or $\mathbf{S}$. Whereas temporal smoothing increases the inter-block covariance (Eq. (10)) and the covariance of entire time course (Eq. (8)), the eigenvalues of the matrix $\mathbf{Q}^{-1}\mathbf{S}$ will not be affected. It is thus expected that the effect of temporal smoothing has a minimal impact on our analysis.

The above argument holds when the temporal scale of autocorrelation or temporal smoothing is small compared to the duration of task block or the entire experimental duration. There are two time

scales in covariances of TRCA: the task duration for the matrix **S** and the entire experimental duration for the matrix **Q**. If the scale of temporal smoothing increases beyond the duration of task block, the components of **S** matrix will be saturated whereas the components of **Q** matrix will still grow. Therefore, the eigenvalues of the matrix $\mathbf{Q}^{-1}\mathbf{S}$ will become smaller, and some of task-related components might not be able to survive. To summarize, the effect of temporal smoothing will be in effect if the smoothing scale becomes the same order of the task block. This consideration was verified with numerical simulations (Section 3.1.3).

2.5. Task-Distinctive Components

In practical applications such as brain-machine interface and brain decoding (Blankertz et al., 2008), it is often desirable to contrast neuroimaging data obtained in multiple task types. Once components related to each task are extracted, those will be used to infer corresponding cognitive states or to drive external devices such as a robot arm. Here we propose that a simple extension of TRCA can provide the most distinctive feature for binary task classification.

Let us consider two types of tasks, say A and B, which have K_{A} and K_{B} blocks with task periods $t \in \left[t_k^{\mathrm{A}}, t_k^{\mathrm{A}} + T \right]$ $\left(k = 1, \cdots, K_{\mathrm{A}} \right)$ and $t \in \left[t_k^{\mathrm{B}}, t_k^{\mathrm{B}} + T \right]$ $\left(k = 1, \cdots, K_{\mathrm{B}} \right)$, respectively. We construct a component that has maximal covariance between blocks of one task type and minimal covariance between blocks of different task types. As in the previous section, the covariance among task-A blocks

$$C_{kl}^{\mathrm{AA}} = \mathrm{Cov}\left(y^{(k_{\mathrm{A}})}(t), y^{(l_{\mathrm{A}})}(t) \right) = \sum_{i,j} w_i w_j \mathrm{Cov}\left(x_i^{(k_{\mathrm{A}})}(t), x_j^{(l_{\mathrm{A}})}(t) \right) \tag{14}$$

and task-B blocks

$$C_{kl}^{\mathrm{BB}} = \mathrm{Cov}\left(y^{(k_{\mathrm{B}})}(t), y^{(l_{\mathrm{B}})}(t)\right) = \sum_{i,j} w_i w_j \mathrm{Cov}\left(x_i^{(k_{\mathrm{B}})}(t), x_j^{(l_{\mathrm{B}})}(t)\right) \tag{15}$$

are to be maximized to give a task-related signal for both tasks A and B. We also require minimizing the covariance between task A and task B blocks,

$$\hat{C}_{kl}^{\mathrm{AB}} = \mathrm{Cov}\left(y^{(k_{\mathrm{A}})}(t), y^{(l_{\mathrm{B}})}(t)\right) = \sum_{i,j} w_i w_j \mathrm{Cov}\left(x_i^{(k_{\mathrm{A}})}(t), x_j^{(l_{\mathrm{B}})}(t)\right) \tag{16}$$

and

$$\hat{C}_{kl}^{\mathrm{BA}} = \mathrm{Cov}\left(y^{(k_{\mathrm{B}})}(t), y^{(l_{\mathrm{A}})}(t)\right) = \sum_{i,j} w_i w_j \mathrm{Cov}\left(x_i^{(k_{\mathrm{B}})}(t), x_j^{(l_{\mathrm{A}})}(t)\right). \tag{17}$$

Accordingly, the linear weighted sum that maximizes the intra-task covariances (Eqs. (14) and (15)) and minimizes the inter-task covariances (Eqs. (16) and (17)) will give the most distinctive time course between the two tasks. For this purpose, the objective function to be maximized now becomes

$$\sum_{\substack{k,l=1 \\ k \neq l}}^{K_{\mathrm{A}},K_{\mathrm{B}}} \left(\hat{C}_{kl}^{\mathrm{AA}} + \hat{C}_{kl}^{\mathrm{BB}}\right) - \sum_{k,l=1}^{K_{\mathrm{A}},K_{\mathrm{B}}} \left(\hat{C}_{kl}^{\mathrm{AB}} + \hat{C}_{kl}^{\mathrm{BA}}\right) = \mathbf{w}^{\mathrm{T}}\mathbf{S}\mathbf{w}\,, \tag{18}$$

where the components of the matrix **S** is defined as

$$\begin{aligned}\left(\mathbf{S}\right)_{ij} \equiv & \sum_{k\neq l}\left[\mathrm{Cov}\left(x_i^{(k_\mathrm{A})}(t), x_j^{(l_\mathrm{A})}(t)\right)+\mathrm{Cov}\left(x_i^{(k_\mathrm{B})}(t), x_j^{(l_\mathrm{B})}(t)\right)\right] \\ & -\sum_{k\neq l}\left[\mathrm{Cov}\left(x_i^{(k_\mathrm{A})}(t), x_j^{(l_\mathrm{B})}(t)\right)+\mathrm{Cov}\left(x_i^{(k_\mathrm{B})}(t), x_j^{(l_\mathrm{A})}(t)\right)\right]\end{aligned}. \tag{19}$$

With this newly defined matrix **S**, the coefficients are determined by solving the Rayleigh-Ritz problem (Eq. (12)), and corresponding components are referred to as task-distinctive components.

2.6. Data Augmentation

The basic formulation of TRCA makes use of multi-channel signals obtained from a single modality, and task periods of a single task. In this sense, TRCA may be considered as a least supervised method. When additional, independent sources of information (such as body movement or respiration signals) are provided, it is desirable to make use of those sources in order to improve the task consistency. Here we show that a simple extension of TRCA can incorporate other sources of task-related and task-unrelated information step by step.

Suppose that, in addition to *N*-channel temporal signals denoted by $x_i(t)$ $\left(i=1,\cdots,N\right)$, additional, independent $\tilde{N}$ temporal signals denoted by $\tilde{x}_i(t)$ $\left(i=1,\cdots,\tilde{N}\right)$ are given. These signals may, for example, represent task-unrelated artifacts such as body movement measured by an accelerometer or respiration measured by a respiratory belt, and we assume that $x_i(t)$'s are corrupted linearly by $\tilde{x}_i(t)$'s. Task consistency can be improved by appropriately subtracting task-unrelated components from $x_i(t)$. We propose that these two sets of temporal signals are augmented to form a new vector **X**:

$$\mathbf{X}\left(t\right)=\left[x_1\left(t\right) \quad \cdots \quad x_N\left(t\right) \quad | \quad \tilde{x}_1\left(t\right) \quad \cdots \quad \tilde{x}_{\tilde{N}}\left(t\right)\right]^T. \tag{20}$$

If we replace the original vector **x** in Eq. (5) with this augmented vector, task-related components can be computed as in Section 2.2. The additional signals provided by $\{\tilde{x}_i(t)\}$ can be regarded as supervised signals, so TRCA has a flexibility of incrementally integrating potentially informative signals.

2.7. Mapping of a Task-Related Component

Once a statistically significant task-related component $y(t)$ is identified, the next task is to evaluate how each time course contains that task-related component. If input time courses are normalized to one, the correlation coefficient between i-th input time course and the task-related component is given as

$$\mathrm{E}\left[x_i(t)\cdot y(t)\right]. \tag{21}$$

By spatially aligning these dot products, a spatial map of the task-related component is obtained for individual subjects. Finally, spatial maps for multiple subjects are averaged channel by channel to obtain a subject-averaged spatial map.

2.8. Application to Synthetic Data

We have conducted four numerical simulations with synthetic data in order to illustrate how TRCA works: (1) a hemodynamic response corrupted with a physiological artifact and a motion artifact with large discontinuity (Section 3.1.1), (2) multiple task-related responses corrupted with physiological artifacts (Section 3.1.2), (3) decorrelation of two-task signals (Section 3.1.3), and (4) incorporation of other source signals for artifact removal (Section 3.1.4). These simulations were designed mainly for the following application to NIRS data. Details of synthetic data are summarized in Appendix B and Table 2. Whereas actual task periods were 30 seconds, extra five seconds prior to a block and 20 seconds after a block (therefore, totally 55 seconds) were included to compute

correlation coefficients and covariances. This will ensure that task-related components have consistent signals not only during but also shortly before and after a task block.

2.9. NIRS Finger Tapping Experiment

Although NIRS measures hemodynamic responses evoked by underlying neural responses like fMRI, the signal-to-noise ratio of NIRS is generally no better than that of fMRI (Cui et al., 2011). Also, NIRS data is corrupted with various systemic noises such as cardiac and respiratory signals, skin blood flow, and motion artifacts (Katura et al., 2006; Sato et al., 2006).

TRCA was then applied to NIRS data set of 29 subjects performing a finger tapping task, which was composed of five blocks, 30 seconds each. Details of experimental data were summarized in our previous publication (Sato et al., 2005; Katura et al., 2008). As in the synthetic case, five seconds before and 20 seconds after the task period were combined for the computation of correlation coefficients and covariances. Amplitudes of NIRS signals considerably vary channel-to-channel, so the standard deviation of each channel time course was normalized to one before applying TRCA. For the analysis of task-related components (Section 3.2.1), the oxy-hemoglobin data for left- and right-finger tapping were analyzed independently. For the analysis of task-distinctive components (Section 3.2.2), the data for left- and right-finger tapping were merged together as if they formed a single measurement, and both oxy- and deoxy-hemoglobin data were used.

2.10. Additional simulations and analyses

In order to assess the performance of our method, several additional simulations were performed with synthetic data with variable activation amplitudes, activation onsets, and sampling rates. Moreover, the method was tested with time courses of a simulated experiment of event-related

design. Also, in order to evaluate how robust task-related components were, TRCA was applied to NIRS data with reduced number of task blocks or channels. These results are summarized in Supplementary Material.

3. RESULTS

3.1. Synthetic Data

Four numerical experiments were conducted to assess our proposed method: Removal of motion artifact (Section 3.1.1), extraction of multiple task-related components (Section 3.1.2), effect of temporal smoothing (Section 3.1.3), distinctive components (Section 3.1.4), and data augmentation (Section 3.1.5). Throughout the main text of this paper, TRCA was formulated and tested in a block-design experiment with non-overlapping task periods. An application to experiments of event-related design with overlapping task-related responses is argued in Supplementary Material.

3.1.1. Removal of motion artifact

Although NIRS is relatively tolerant to head and body movements compared to other neuroimaging modalities such as fMRI, its data still suffers from motion artifacts (Sato et al., 2006; Cui et al., 2010). In order to address how TRCA works for motion-contaminated data, synthetic data was created with a single task-related component and physical and physiological task-unrelated components (Figure 3A). For the task-related component, five blocks of 30 seconds were included, and expected activations were computed by convolving with a standard hemodynamic response function (Boynton et al., 1996). The signals in Figure 3A were randomly mixed to generate synthetic NIRS signals in Figure 3B. An obvious jump at 315 seconds during the third block indicates that simple block averaging cannot remove such a large discontinuity.

We then applied TRCA to the synthetic data. The correlation matrices, $\mathbf{S}$ and $\mathbf{Q}$, were

computed by their definitions (Eqs. (11) and (8)). **Y** contains possible task-related components. We emphasize that the eigenvalues are the task consistency (Eq. (13)) of corresponding components. In other words, the reproducibility of a task-related component can be quantified by the corresponding eigenvalue.

Figure 3C shows reconstructed task-related components in the order of decreasing eigenvalues. A statistical test indicated that only one component was statistically significant (Figure 3E); the top row denotes task-related component with the largest eigenvalue, and clearly this component recovered the hemodynamic response and did not suffer from the large discontinuity at 315 seconds. The other components were the jump and the physiological component, respectively, which are not regarded as task related due to their eigenvalues within the chance interval. Figure 3D illustrates independent components computed by using the JADE algorithm (Cardoso, 1999). The jump component, hemodynamics component, and physiological component were separated, but an additional analysis step was needed to determine which component was task-related and task-unrelated.

3.1.2. Extraction of multiple task-related components

Generally the eigenvalue problem of Eq. (12) gives N possible solutions, and their task relatedness needs to be assessed by a statistical test on corresponding eigenvalues. By counting the number of statistically significant eigenvalues, therefore, the number of latent, task-related components can be estimated. Two task-related components and one task-unrelated component (Figure 4A) were used to create synthetic data (Figure 4B). Correspondingly, three potential task-related components were obtained (Figure 4C). Their statistical significance was assessed by comparing with eigenvalues computed from block-shuffled inputs. There was one eigenvalue inside the confidence interval, and there were two eigenvalues outside the confidence interval (Figure 4D), thereby successfully recovering the original two task-related components and rejecting the remaining

one as task-unrelated.

3.1.3. Effect of temporal smoothing

Whereas autocorrelation in time series reduces the noise variance and thus GLM analyses require an appropriate correction for the statistic, in Section 2.4 we provided an intuitive explanation of why autocorrelation will not matter in the case of TRCA, on condition that the time constant of autocorrelation is small compared with the duration of task block. To verify this intuition, a numerical simulation was performed by controlling the degree of autocorrelation with temporally smoothed synthetic data of various time scales. Five synthetic time courses were created from two task-related components corrupted with three task-unrelated components (see Section 1.3 of Supplementary Material for details), followed by temporal smoothing with Gaussian window of three values for full-width half-maximum or FWHM (1, 10, or 30 seconds) (Figures 5A-C). In this simulation, the duration of task block was 30 seconds, followed by 70 seconds of rest, thereby consisting of a periodic block design of 100 seconds. Details observed in the time courses in panel (A) became less apparent with the increase of the smoothing scale. For the three sets of data, the resampling distributions indicated that the two task-related components were correctly identified for the cases of 1 and10 second FWHMs (Figures 5D and 5E), whereas only one component was recovered for the case of 30 second FWHM (Figure 5F), as expected from our intuitive explanation. Corresponding task-related components were shown in Figures 5H-I. With the consideration in Section 2.4 supported by this numerical result, we conclude that TRCA can safely be applied to data with considerable temporal autocorrelation if the scale of temporal autocorrelation is shorter than the duration of task block. This result also suggests that, if data contains autocorrelation due to hemodynamic response or temporal smoothing, the task duration used for TRCA should be set sufficiently longer than the scale of autocorrelation, as discussed in designing an fMRI experiment (Friston et al., 2000).

3.1.4. Task-distinctive component

Often it is desirable to contrast activations from two distinct tasks, so synthetic data was created that contained two independent activations of two tasks (Figure 6A). TRCA was applied to differentiate synthetic time courses that were composed of task-related components of two distinct tasks (Figure 6B). A solution with the highest eigenvalue contained increases during blocks of one task and decreases during blocks of another task (Figures 6C and 6D). Intra-task correlations were 0.93 (SD 0.0084) and 0.92 (SD 0.016) for task A and task B, respectively, and an inter-task correlation was -0.93 (SD 0.018).

3.1.5. Incorporation of augmented signals

In some cases in which signals and artifacts are mixed by a similar proportion to multiple time series, simple summation or subtraction between multiple time series cannot entirely cancel artifacts. Often additional sources of potential artifacts can be obtained by a separate and simultaneous recording such as cardiac, respiratory or motion measurements. TRCA is able to flexibly incorporate additional sources of artifact related components. Synthetic data was constructed from three signal time courses (Figure 7A), and three random mixtures were used as inputs to TRCA (Figure 7B, top three). Also, additional time course of a sudden jump was assumed (Figure 7B, bottom). When only the three mixed time courses were used, often the discontinuity was not totally removed (Figure 7C, top). This failure occurred when the individual time courses (top three in Figure 7B) happened to contain hemodynamics and jump components in similar proportions. In contrast, TRCA applied to the augmented data could remove the jump component completely (Figure 7C, bottom). The performance of the non-augmented and augmented methods was assessed by repeating this simulation with randomized mixture coefficients for one thousand times and by computing a baseline-change index defined by:

$$\frac{\text{mean}\left[y(t)\Big|_{t=315}^{t=600} \right]\text{-mean}\left[y(t)\Big|_{t=0}^{t=315} \right]}{\text{std}\left[y(t)\Big|_{t=0}^{t=600} \right]} \quad (22)$$

.

The index takes zero if the jump component is completely removed. Figure 7D shows a box plot of the indices, indicating that the performance of TRCA can be improved by incorporating additional sources of artifact information.

3.2. NIRS Data of Finger Tapping

3.2.1. Task related components

An example of artifact removal is shown in Figure 8. Time courses of six channels with largest correlation coefficients out of 24 channels (Subject #23, left finger tapping) contain several artifacts that appeared to originate from body movements (Figure 8A). These components occurred not reproducibly between task blocks, so TRCA optimized the weight coefficients so as to suppress these artifacts. The dominant TRC with the largest eigenvalue did not suffer these artifacts (Figure 8B). Note also that there was an improvement in the correlation coefficient; the largest correlation coefficient among individual channels was 0.45 (top left in Figure 8A), and the correlation coefficient of the dominant task-related component was 0.86. Also, this TRC appeared consistent with known properties of hemodynamic response in the motor cortex (Rao et al., 1996).

The same analysis was applied to all subjects. The numbers of statistically significant task-related components ranged from zero to three (Table 1). Most subjects had one or two components. There were a total of 99 task-related components (49 and 50 for right- and left-finger tapping) that were statistically significant. Since most subjects had at most two components, a *k*-means cluster analysis (k=2) with respect to Euclidean distance was performed in order to classify these dominant components.

# Statistically significant components	# Subjects (left-finger tapping)	# Subjects (right-finger tapping)
0	1	1
1	8	6
2	19	22
3	1	0

Table 1. Numbers of statistically significant task-related components for left- and right-finger tapping experiment.

Figure 9 summarizes the two dominant TRCs for right-finger tapping. One TRC had a gradually changing time course similar to a conventional hemodynamics response; it gradually increased a few seconds after the task onsets and decreased a few seconds after the task offsets (Figure 9A). Another TRC had a piece-wise linear time course; it peaked after a few seconds after the task onsets, linearly decreased until a few seconds after the task onsets, and then increased linearly (Figure 9C). The inter-block correlations were 0.74 (SD 0.18) (Figure 9A) and 0.56 (SD 0.17) (Figure 9C), respectively. To visualize the contribution of the task-related components with the highest eigenvalues to original NIRS signals, projection coefficients (defined by a dot product $v_i = \mathrm{E}\left[y(t) \cdot x_i(t) \right]$, see Section 2.7) were first computed for individual subjects and then averaged over all subjects. One TRC projection map showed laterality to the contralateral hemisphere (Figure 9B), whereas the other TRC map appeared to spread over the both hemispheres (Figure 9D). We computed a laterality index (LI) defined by

$$\mathrm{LI} = \left(\sum_{i \in \substack{\text{Left} \\ \text{Hemiphere}}} v_i - \sum_{i \in \substack{\text{Right} \\ \text{Hemiphere}}} v_i \right) \Big/ \sum_i |v_i| \tag{20}$$

which takes a positive or negative value for left- or right-hemisphere dominant activation, respectively. Laterality indices were 0.17 (SD 0.30) and -0.0010 (SD 0.23) for Figures 9B and 9D, respectively.

Similarly, Figure 10 summarizes the two dominant TRCs for left-finger tapping. The inter-block correlations were 0.75 (SD 0.16) (Figure 10A) and 0.63 (SD 0.16) (Figure 10C), respectively. As in the case of the right-finger tapping, one component showed contralateral dominance (Figure 10B) while another component appeared in both hemispheres (Figure 10D). The laterality indices were -0.20 (SD 0.24) (Figure 10B) and 0.060 (SD 0.28) (Figure 10D), respectively. Furthermore, in order to see how robustly TRCA could detect these two dominant TRCs, TRCA was applied to a dataset with the reduced number of task blocks or NIRS channels. We found that TRCA could recover the two components robustly (see Supplementary Figures 5 and 6).

The performance of the CovMax and CorrMax algorithms was evaluated by inter-block correlation coefficients. For comparison, correlations of all individual channels (29 (subjects) ×24 (channels) ×2 (conditions)) were computed. Medians of all individual channels, channels with maximal correlation per subject, and task related components derived by the CovMax and CorrMax algorithms were: 0.17, 0.50, 0.76 and 0.83 for left-finger tapping, and 0.18, 0.55, 0.71 and 0.85 for right-finger tapping. Computational time of the CovMax algorithm was 0.48 (SD 0.013) seconds per subject, and that of the CorrMax algorithm was 4.36 (SD 1.5592) seconds (Matlab 2011b, Intel Core2Duo CPU 3.0 GHz).

3.2.2. Task-distinctive component

A task-distinctive component was extracted from right- and left-finger tapping data by using the algorithm presented in Section 2.4. Figure 11A shows a representative time course from a single subject (Subject #12), and Figure 11B shows its block averages. Correlations between blocks of one task type (intra-task correlation) for this subject were 0.84 (SD 0.038) and 0.86 (SD 0.056) for left- and right-finger tapping, respectively, and correlation between blocks of different task types (inter-task correlation) was -0.85 (SD 0.044). In Panel B, blocks of left-finger tapping showed elevated activations (blue lines) whereas blocks of right-finger tapping showed depressions (red lines). A group average of the same analysis was shown in Figure 11C; Intra-task correlations for all subjects were 0.53 (SD 0.25) and 0.50 (SD 0.27) for left- and right-finger tapping, respectively, and an inter-task correlation was -0.50 (SD 0.26). A projection map of this task-distinct component averaged all subjects is illustrated in Figure 11D.

The task-distinctive components provide a succinct description to classify two tasks from physiological measurements. NIRS has an advantage of simultaneous recording of oxy- and deoxy-hemoglobin, so TRCA was applied to both oxy- and deoxy-hemoglobin signals. Figure 12A shows two task-distinctive components from the same subject in Figure 11. The time courses of these task-distinctive components were projected onto a two-dimensional plane composed of oxy- and deoxy-hemoglobin signals (Figure 12B). One sees that left- and right-finger tapping signals were inseparable before and after task period and separable during task period, indicating that these task-distinctive components provide a low-dimensional representation for classifying cognitive states. The same analysis was applied to all subjects (Figure 12C).

4. DISCUSSION

An analysis method based on inter-block reproducibility of biophysical signals was proposed. The reproducibility of signals among task blocks was measured with a sum of correlation

coefficients (Eq. (7)) or covariances (Eq. (10)). In the latter case, the maximization of sum of covariances was reduced to a Rayleigh-Ritz eigenvalue problem, and a statistical significance of task relatedness was quantified by eigenvalues against a null hypothesis. Our task-related component analysis (TRCA) was applied to both synthetic and NIRS data. We demonstrated that TRCA is not sensitive to data with autocorrelation whose time scale is smaller than the duration of task block; this insensitivity to autocorrelation is advantageous when TRCA is generalized to other neuroimaging modalities or biophysical measurements.

4.1. Comparison with Previous Approaches

Several comments are made on this analysis method in comparison with previous approaches to neuroimaging data. First, this method differs from traditional, single-channel based analysis such as general linear models (Friston et al., 1994b), in which task related components are extracted within a single-channel time course. General linear models (GLMs) decompose individual voxel time courses into several presumed components, and the contribution of each component is assessed statistically. This approach implicitly assumes the fact that whole brain areas are entirely and uniformly sampled so GLMs should be able to detect task related voxels if there are any. These assumptions, however, may not hold for other functional neuroimaging modalities such as NIRS and EEG, whose sampling points are sparsely located only on the scalp. Our method, on the contrary, attempts to reconstruct a task related component from multiple-channel time courses with appropriate weight coefficients, and cortical areas responsible for the task consistency are mapped by evaluating a correlation between a task-related and original time courses. Also, the GLM approach depends critically on hypotheses of contributing time courses such as a shape of hemodynamic response (Plichta et al., 2007). On the other hand, our TRCA requires only onset timings of task blocks but not detailed time courses.

Second, the proposed method is, in mathematical formulation, similar to periodic component analysis, which is also formulated as a Rayleigh-Ritz eigenvalue problem (Saul and Allen, 2001; Sameni et al., 2008; Monasterio et al., 2010). We note, however, that our method is not restricted to periodic signals as long as task onsets are known, so it is flexibly applicable to an experimental design which uses non-periodic task cycles (see an application to event-related experiment in Supplementary Material).

Finally, our proposed analysis is an eigenvalues problem, so extracted components can be obtained with standard linear algebra methods that are computationally inexpensive. Moreover, statistical significance of an extracted component can be assessed by an associated eigenvalue, which implies the degree of inter-block covariances. This makes a contrast with independent component analysis, in which an additional procedure for quantifying how extracted independent components are task related is required. Our previous work applied ICA to the same dataset of finger tapping and found two task-related components that were similar to those reported in this work (Katura et al., 2008). But, in order to identify task-related components among candidate components separated by ICA, a threshold of inter-block correlation (0.2) was imposed, which was determined rather arbitrary by hand. Another ICA study extracted an artifact component possibly related to skin blood flow by introducing an index describing spatial distribution of components (Kohno et al., 2007). They identified the most spatially uniform component as an artifact of skin blood flow, but what degree of uniformity is needed to be identified as such an artifact remains arbitrary. Our proposed method, in contrast, extracted two task-related components without introducing such arbitrary selection parameters.

4.2. Dominant Task-Related Components

Our proposed method discovered statistically significant task-related components. One

component (Figures 8A and 9A) had a gradually changing time course and appeared in the hemisphere contralateral to tapping fingers (Figures 8B and 9B). Therefore, we interpreted this component to be a hemodynamic response to finger tapping execution. Another component (Figures 8C and 9C) had a piece-wise linear time course and its peaks occurred a few seconds after the task onsets. This component did not show a consistent hemispheric localization (Figures 8D and 9D). In conventional NIRS analyses where multi-subject data was averaged on a channel-by-channel basis, this piece-wise linear component was not reported before to our knowledge. This component was not spatially reproducible but temporally reproducible, so the conventional analysis on channel-by-channel basis might not be able to detect this component. Our proposed TRCA based on temporal reproducibility could discover it.

One then will ask what this piece-wise component might represent. One interpretation is that it represents variable delays of hemodynamic responses in individual channels. Interestingly, we noticed that the temporal derivative of the hemodynamic response conspicuously resembled the piece-wise component (Supplementary Figures 7A and 7B). In GLM analyses for fMRI data, it is a common practice to include a hemodynamic time course along with its temporal derivative so that delays in individual activations are adjusted. Although this may explain certain delays in activation onsets, we found that raw time courses of some channels closely resembled this piece-wise linear component (Supplementary Figure 7C). Therefore, the delay interpretation itself cannot explain this piece-wise linear component.

Another interpretation of this component is hemodynamic fluctuations in the scalp that are estimated to be 10 to 20 times higher than those in cortical layers (Takahashi et al., 2011). There is considerable interest in the NIRS community in understanding hemoglobin changes that originate from neural and from systemic activities such as heart rate or blood pressure (Tachtsidis et al., 2009; Tachtsidis et al., 2010; Patel et al., 2011). Recently, (Kirilina et al., 2012) reported oxy-hemoglobin

time courses similar to our piece-wise linear component in a continuous performance task and a n-back working memory task. Functional NIRS combined with fMRI and peripheral physiological measurements revealed that these time courses were systemic artifacts whose origin was a task-evoked sympathetic arterial vasoconstriction followed by a decrease in venous volume in the scalp. In one study, (Minati et al., 2011) quantified, with shallow- and deep-penetrating NIRS recording, the contribution of systemic blood pressure changes caused transiently by arm raising and concluded that systemic changes were reflected both in intra- and extra-cranial signals but with different patterns. In a related study, (Saager et al., 2011) used two-detector NIRS with short and long separations and improved the signal-to-noise ratio by subtracting short-separation components from long-separation components.(Takahashi et al., 2011) quantified the contribution of skin blood flow changes confounding in NIRS signal during a verbal fluency task by applying a pressure on the scalp between transmitting and detecting optodes. These studies employed certain specialized experiment settings such as two-distance optodes or pressure gauge, so it would be more convenient if confounding signals originating from systemic factors are identified and separated by a signal processing method.

To demonstrate this more explicitly, TRCA was applied to deoxy-hemoglobin as well as oxy-hemoglobin data. A recent study (Cui et al., 2010) suggested an artifact removal method based on the fact that the concentration changes of oxy- and deoxy-hemoglobin are negatively correlated for neural activation but not so for motion artifacts. We followed the same reasoning; if one component from oxy-hemoglobin is negatively correlated with another component from deoxy-hemoglobin, they are likely related to neural activation. Otherwise, positively or weakly correlated components are likely non-neural artifacts. We thus applied TRCA to deoxy-hemoglobin data (data not shown). One TRC in oxy-hemoglobin was negatively correlated with another TRC in deoxy-hemoglobin, therefore suggesting their neural origin. In contrast, one TRC in oxy-hemoglobin

was positively correlated with another TRC in deoxy-hemoglobin, thereby indicating that they were not from neural activation. Thus TRCA can be a tool for separating components related to neural activation from those related to systemic factors.

We would like also to point out that a time course similar to ours was reported in a multi-wavelength intrinsic optical imaging experiment in which behaving animal performed a visual attention task (Sirotin and Das, 2009; Sirotin et al., 2012) (there is, however, a controversy over whether or not the component Sirotin and Das reported was really task anticipatory and whether this component could be explained by electrophysiological signals, see (Kleinschmidt and Muller, 2010; Das and Sirotin, 2011; Handwerker and Bandettini, 2011b, a)). Given the facts that the subjects were instructed that our task design was repetitive before the experiment (thus anticipatory) and that NIRS uses multiple wavelengths (thus containing information of not only oxygenation but also blood volume), it might not be surprising that NIRS signals contained some anticipatory signals similar to what Sirotin and Das had reported.

4.3. Possible Extensions and Future Applications

This paper provided the basic formulation of task-related component analysis, and a few theoretical and practical extensions are considered here. First, whereas this paper proposed temporally reproducible signals as task-related components, spatially reproducible signals can also be considered as being task related. TRCA can be formulated so that an activation map has a maximal covariance between task blocks. Spatial TRCA may be applicable to fMRI data, in which temporal dimension (the number of temporal samplings) is usually much smaller than spatial dimensions (the number of voxels).

In our basic formulation of TRCA, the objective functions (Eqs. (7), (9) and (19)) contain the contributions of successive blocks and distant blocks equally, namely that the covariances between

successive blocks and between distant blocks have the same weights in the objective functions. The assumption of our method is that components that are task-related should appear in the same manner in every task block, so in the basic formulation of our method the effect of changing hemodynamic responses in the course of experiment has not been modeled. These equal contributions may be justified when no changes in activation during the course of experiment are expected, as in simple tasks such as finger tapping. It is, however, desirable to extract adaptive changes of activation profiles during the course of experiment, such as those related to learning or habituation. One way to model such effects could be introduce additional factor to account the duration of experiment:

$$\sum_{\substack{k,l=1 \\ k\neq l}}^{K} f_{kl}\,\mathrm{Cov}\left(y^{(k)}(t), y^{(l)}(t)\right) \tag{21}$$

If the factor (f_{kl}) is a decreasing function of the block distance $|k-l|$, the covariance between initial blocks and late blocks becomes less important. Therefore, the signals from initial and late blocks are not required to be very similar; only gradually signals that change block-by-block will be extracted.

Throughout this paper, we restrict ourselves to a linear model (Eq. (5)) to maximize the inter-block correlation or covariance. Higher reproducibility may be expected if input signals are mapped into a high dimensional feature space. A nonlinear extension may be possible by applying a kernel method, which has proved to be useful in areas such as kernel PCA (Mika et al., 1999b), kernel ICA (Bach and Jordan, 2003), kernel discriminant analysis (Mika et al., 1999a). Particularly, our linear formalism shares the same mathematics with Fisher linear discriminant analysis, so it is readily extendable to a nonlinear formalism with the help of kernel methods.

TRCA can also be applicable to multi-channel data that have several behaviorally relevant onsets. For example, a typical working-memory task contains stimulus-presentation timings and response timings of subjects. TRCA with stimulus-onsets and with response-onsets may reveal stimulus- and response-related activations, respectively. Our future study will address these

limitations and extensions of TRCA.

Acknowledgments

We thank Drs. Naoki Tanaka and Masashi Kiguchi for encouraging discussions, Dr. Aniruddha Das for his help regarding the interpretation of NIRS signals, and three anonymous reviewers for their thoughtful comments. Thanks also go to Dr. Terrence J. Sejnowski for his comments on applications of independent component analysis to neuroimaging data. We acknowledge that Dr. Hiroshi Imamizu provided insightful comments on an earlier version of this manuscript.

Appendix A: MATLAB code

```
function [Y, V, D, S, C] = TRCA(X, t1, Nexp)


%% task-related component analysis
% Covariance Maximization (CovMax) algorithm
% X: data matrix (N channels * T time points)
% t1: task onsets (vector)
% Nexp: task duration (sampling unit)

Nchannel = size(X, 1);
Nblock = length(t1);

% computation of correlation matrices:
 S = zeros(Nchannel, Nchannel);
 for i=1:Nchannel
       for j=1:Nchannel
             for k=1:Nblock
                   for l=1:Nblock
                         if k~=l
                               tk = t1(k); %onset of l-th block
                               tl = t1(l);    %onset of l-th block
                               xi = X(i, tk:tk+Nexp);
                               xj = X(j, tl:tl+Nexp);
                               S(i,j) = S(i,j) + (xi-mean(xi,2))*(xj-mean(xj,2))';
                         end
                   end
             end
       end
 end

X = X – repmat(mean(X,1),1,size(X,2));
Q = X*X';

% TRCA eigenvalue algorithm
[V, D] = eig(Q\S);
Y = V'*X;
```

Appendix B: Synthetic Data

Here we describe some details of how synthetic data **X** was created for the four simulations in Section 3.1. **X** represents an N (# channels) $\times T$ (# time points) matrix. N_s source signals were created and compiled into an $N_s \times T$ matrix **R**. These source signals could be task-related (i.e., hemodynamic responses) or -unrelated (i.e., systemic or movement-related artifacts). As in Section 2.1., these source time series were randomly mixed up to give six synthetic time series (**X**: N (# channels) * T (# time points)) as

$$\mathbf{X} = \mathbf{AR} + \boldsymbol{\xi}, \tag{B.1}$$

where **A** is the $N \times N_s$ mixing matrix. A Gaussian noise vector $\boldsymbol{\xi}$ of mean 0 and variance 0.3 was added. All time courses were sampled at 10 Hz. The four simulations (Sections 3.1.1 – 3.1.4) differed in how the matrices **R** and **A** were created. Details of how the four synthetic data sets used in the main texts are summarized below and in Table 2.

Simulation in Section 3.1.1: One hemodynamic response (r_1), one physiological component (r_3), and physical jump component (r_4) formed the matrix **R**.

$$\mathbf{R} = \begin{bmatrix} r_1 & r_3 & r_4 \end{bmatrix}^{\mathrm{T}} \tag{B.2}$$

These time courses were 600 second long and sampled with 10 Hz (therefore, T=600). For hemodynamic response (r_1), five task blocks of 30 seconds were placed at 100, 200, 300, 400 and 500 seconds, and a box-car function ($s(t)$) was defined to be one during the task periods and zero otherwise. A hemodynamic response function was adopted from Boynton et al. (1996):

$$h(t) = \left(\frac{t}{\tau}\right)^{n-1} \exp\left(-\frac{t}{\tau}\right) \Big/ (n-1)!\,\tau \tag{B.3}$$

where τ=1.08 and n=3. Hemodynamic response (hence task related) were computed by convolving $\underline{s}(t)$ and $h(t)$. For physiological component (r_3), an oscillatory signal of 0.0833 Hz (or 12 second period) was included to emulate the Mayer wave. For a physical artifact (r_4), a large jump at 315

second was included to emulate a motion artifact. The 3×3 mixing matrix **A** was created as

$$\mathbf{A}=\begin{pmatrix}1&0&3\\1&0&3\\1&0&3\end{pmatrix}+\begin{pmatrix}\eta_{11}&\eta_{12}&\eta_{13}\\\eta_{21}&\eta_{22}&\eta_{23}\\\eta_{31}&\eta_{32}&\eta_{33}\end{pmatrix} \tag{B.4}$$

where $\eta \sim N\left(0,0.5^2\right)$.

Simulation in Section 3.1.2: Five task blocks were included as in the simulation in Section 3.1.1. In addition to the sustained hemodynamic response function (r_1), another, transient task-related component (r_2) was introduced as a temporal derivative of Eq. (B.3). This phasic component was responsive positively to onset and negatively to offset of a task. The Mayer wave was also included, and the matrix **R** was defined as

$$\mathbf{R}=\left[r_1(t)\quad r_2(t)\quad r_3(t)\right]^{\mathrm{T}}. \tag{B.5}$$

The 3×3 matrix **A** was created as

$$\mathbf{A}=\begin{pmatrix}0.5&0.5&0\\0.5&0.5&0\\0.5&0.5&0\end{pmatrix}+\begin{pmatrix}\eta_{11}&\eta_{12}&\eta_{13}\\\eta_{21}&\eta_{22}&\eta_{23}\\\eta_{31}&\eta_{32}&\eta_{33}\end{pmatrix}, \tag{B.6}$$

where $\eta \sim N\left(0,0.5^2\right)$.

Simulation in Section 3.1.3: Ten task blocks, five for task A and other five for task B, were created alternately from 100 to 1000 in step of 100 seconds. The total duration was 1200 seconds sampled at 10 Hz. Two tasks were inserted alternatively; five task-A blocks of 30 seconds were placed starting at 100, 300, 500, 700 and 900 seconds, and five task-B blocks of 30 seconds starting at 200, 400, 600, 800 and1000 seconds. Accordingly, two box-car functions were constructed, and corresponding hemodynamic responses (r_1^{A} and r_1^{B}) were then created by convolving the box-car functions and Eq. (B.3). The Mayer-wave component was also added. The matrix **R** was

$$\mathbf{R} = \left[r_1^{\mathrm{A}}(t) \quad r_1^{\mathrm{B}}(t) \quad r_3(t) \right]^{\mathrm{T}}, \tag{B.7}$$

and the 4×3 matrix **A** was

$$\mathbf{A} = \begin{pmatrix} 1.0 & 0.2 & \eta_{13} \\ 0.8 & 0.4 & \eta_{23} \\ 0.6 & 0.6 & \eta_{33} \\ 0.4 & 0.8 & \eta_{43} \\ 0.2 & 1.0 & \eta_{53} \end{pmatrix}, \tag{B.8}$$

where $\eta \sim N\left(0, 0.3^2\right)$.

Simulation in Section 3.1.4: A data matrix composed of three time courses in Figure 7B (top three) was created as in the same way of Section 3.1.1. In addition, an augmented data matrix composed of the three time courses plus one movement time course was created as:

$$\mathbf{X}(t) = \left[x_1(t) \quad x_2(t) \quad x_3(t) \quad r_4(t) \right]^{\mathrm{T}}. \tag{B.9}$$

Notation	Signal type	Functional form
$r_1(t)$	**Sustained hemodynamic response (task-related)**	$s * h(t)$
$r_2(t)$	**Transient hemodynamic response (task-related)**	$\frac{d}{dt} s * h(t)$
$r_3(t)$	**Mayer wave (task-unrelated)**	$A_{\mathrm{M}} \sin\left(\frac{2\pi t}{T_{\mathrm{M}}}\right)$ $\left(A_{\mathrm{M}} = 0.5,\ T_{\mathrm{M}} = 12\right)$
$r_4(t)$	**Sudden discontinuity (task-unrelated)**	$\Theta(t-315) = \begin{cases} 1 & (t > 315) \\ 0 & (t \le 315) \end{cases}$

Table 2: Task-related and –unrelated components that were used for synthetic data.

Figure Legends

Figure 1: (A) Time courses of task-related ($s(t)$) and task-unrelated ($n(t)$) components. Blue shaded areas indicate task blocks, and $s^{(i)}$ and $n^{(i)}$ are i-th block segments of $s(t)$ and $n(t)$, respectively. (B) A generative model of observation ($x_1(t)$ and $x_2(t)$) from task-related ($s(t)$) and task-unrelated ($n(t)$) components. (C) Schematics of TRCA. Multiple time series (left row) are summed with weights to give a single time course $y(t)$ (right). Shaded area in the time series indicate task blocks of a single task. The weights, or coefficients, are determined so as to maximize the sum of correlations or covariances of $y(t)$ between task blocks.

Figure 2: Flow chart of TRCA. (A) Original multi-channel time series are decomposed into (B) task-related components using the algorithm presented in Section 2.2. (C) Statistical significance of the eigenvalues (red crosses on the horizontal axis) is evaluated using the resampling procedure in Section 2.3. The dotted vertical line indicates a 99% confidence level. (D) Two eigenvalues outside the confidence level are selected as being significantly task-related in this case. The framed boxes on the right depict block averages of the two components, respectively. These figures were created with NIRS finger tapping data.

Figure 3: Removal of a large movement artifact. (A) Input synthetic time series (from top to bottom: hemodynamic response, slow wave, and large-amplitude jerky movement). (B) Randomly mixed time courses. The red lines at 315 seconds during the third block indicate the moment of the sudden, large discontinuity. (C) Task related components with corresponding eigenvalues in a descending order and (D) independent components computed with the JADE algorithm. The components in Panels (C) and (D) were moving averaged with a

temporal window of one second after applying TRCA and JADE algorithms, respectively. (E) Eigenvalue distribution computed with randomized task onsets (gray bars) and original eigenvalues (red crosses). The vertical dashed line indicates 99% confidence interval.

Figure 4: Extraction of multiple task related components. (A) Input synthetic time series (from top to bottom: two task-related and one task-unrelated components). (B) Randomly mixed time courses. (C) Task-related components with corresponding eigenvalues. (D) Eigenvalue distribution computed with randomized task onsets (blue bars) and original eigenvalues (red crosses). The vertical dashed line indicates 99% confidence interval.

Figure 5: Effect of temporal smoothing. (A, B, C) Input time courses smoothed with a Gaussian window of 1, 10 and 30 second FWHMs, respectively. (D, E, F) Eigenvalue distributions using randomized task onsets from the data in panel A, B and C, respectively. The red crosses on the horizontal axis represent the eigenvalues computed with the actual task onsets. The numbers indicate the corresponding components shown below in panels G, H or I. The asterisks denote statistical significance ($p<0.01$). (G, H, I) Extracted task-related components.

Figure 6: Discriminative signal computed by TRCA. (A) Two task-related hemodynamics (top two) and task-unrelated slow wave (bottom). Blue- and red-shaded areas suggest task-A and task-B periods, respectively. (B) Five randomly mixed signals. (C) Most distinctive component and (D) its block averages.

Figure 7: Data augmentation in TRCA. (A) Three synthetic signals used for the simulation. (B) Randomly mixed signals (top three) and motion related signals (bottom). (C) Task-related component with the highest eigenvalue when the top three signals (top) or all the four signals (bottom) were used. (D) Box plot of the baseline-change indices of one-thousand repeated simulations.

Figure 8: Motion artifact removal by TRCA. (A) Time courses of NIRS channels with six largest inter-block correlation coefficients out of 24 channels. The numbers in upper left corners are corresponding correlation coefficients. Some artifacts that were possibly caused by body movements are indicated by blue arrows around 155 seconds and red arrows around 303 seconds. (B) Task-related component with the largest eigenvalue. The number at the upper left corner is a correlation coefficient among task blocks.

Figure 9: (A) One TRC of right finger tapping and (B) the corresponding projection map. (C) Another TRC of right finger tapping and (D) the corresponding projection map.

Figure 10: (A) One TRC of left finger tapping and (B) the corresponding projection map. (C) Another TRC of left finger tapping and (D) the corresponding projection map.

Figure 11: (A) The most discriminatory time course computed from a representative subject. Blue and red shaded area denote the task periods of right and left finger tapping, respectively. (B) Task-block average of the time course in panel (A). Thin blue and red lines denote individual right and left finger tapping blocks, respectively, and thick blue and red lines are their averages. (C) Task block average computed from all subjects. Error bars indicate standard

errors. (D) Corresponding project map averaged over all subjects.

Figure 12: (A) Most distinctive time courses computed using oxy- (solid line) and deoxy- (dotted line) hemoglobin NIRS signals of Subject #12. Blue and red shaded area denote the task periods of right and left finger tapping, respectively. (B) Snap shots of the distinctive components in Panel A at t ranging from -5.0 to 40.0 in step of five seconds. The horizontal and vertical axes denote distinctive components constructed from oxy- and deoxy-hemoglobin signals, respectively. Task period was indicated as light-gray background, and rest period as dark-gray background. (C) Snap shots of the distinctive components computed from all subjects at t ranging from -5.0 to 40.0 in step of five seconds, using the same format of panel B. Translucent blue and red circles depict individual blocks, and large solid blue and red circles depict the center of mass.

References

Amari S, Cichocki A, Yang HH (1996) A new learning algorithm for blind signal separation. Advances in Neural Information Processing Systems:757-763.

Bach FR, Jordan MI (2003) Kernel independent component analysis. Journal of Machine Learning Research 3:1-48.

Bell AJ, Sejnowski TJ (1995) An information-maximization approach to blind separation and blind deconvolution. Neural Comput 7:1129-1159.

Blankertz B, Tomioka R, Lemm S, Kawanabe M, Muller KR (2008) Optimizing spatial filters for robust EEG single-trial analysis. Signal Processing Magazine, IEEE 25:41-56.

Boynton GM, Engel SA, Glover GH, Heeger DJ (1996) Linear systems analysis of functional magnetic resonance imaging in human V1. The Journal of Neuroscience 16:4207.

Calhoun VD, Adali T, Stevens MC, Kiehl KA, Pekar JJ (2005) Semi-blind ICA of fMRI: A method for utilizing hypothesis-derived time courses in a spatial ICA analysis. Neuroimage 25:527-538.

Cardoso JF (1999) High-order contrasts for independent component analysis. Neural Computation 11:157-192.

Cui X, Bray S, Reiss AL (2010) Functional near infrared spectroscopy (NIRS) signal improvement based on negative correlation between oxygenated and deoxygenated hemoglobin dynamics. Neuroimage 49:3039-3046.

Cui X, Bray S, Bryant DM, Glover GH, Reiss AL (2011) A quantitative comparison of NIRS and fMRI across multiple cognitive tasks. Neuroimage 54:2808-2821.

Das A, Sirotin YB (2011) What could underlie the trial-related signal? A response to the commentaries by Drs. Kleinschmidt and Muller, and Drs. Handwerker and Bandettini.

Neuroimage 55:1413-1418; discussion 1419-1422.

Fekete T, Rubin D, Carlson JM, Mujica-Parodi LR (2011) The NIRS Analysis Package: noise reduction and statistical inference. PLoS One 6:e24322.

Friston KJ, Jezzard P, Turner R (1994a) Analysis of functional MRI time-series. Human Brain Mapping 1:153-171.

Friston KJ, Holmes AP, Worsley KJ, Poline JP, Frith CD, Frackowiak RSJ (1994b) Statistical parametric maps in functional imaging: a general linear approach. Hum Brain Map 2:189-210.

Friston KJ, Josephs O, Zarahn E, Holmes AP, Rouquette S, Poline J (2000) To smooth or not to smooth? Bias and efficiency in fMRI time-series analysis. Neuroimage 12:196-208.

Friston KJ, Holmes AP, Poline JB, Grasby PJ, Williams SC, Frackowiak RS, Turner R (1995) Analysis of fMRI time-series revisited. Neuroimage 2:45-53.

Handwerker DA, Bandettini PA (2011a) Simple explanations before complex theories: Alternative interpretations of Sirotin and Das' observations. NeuroImage.

Handwerker DA, Bandettini PA (2011b) Hemodynamic signals not predicted? Not so: a comment on Sirotin and Das (2009). Neuroimage 55:1409-1412.

Hyvarinen A, Oja E (1997) A fast fixed-point algorithm for independent component analysis. Neural Comput 9:1483-1492.

Katura T, Tanaka N, Obata A, Sato H, Maki A (2006) Quantitative evaluation of interrelations between spontaneous low-frequency oscillations in cerebral hemodynamics and systemic cardiovascular dynamics. Neuroimage 31:1592-1600.

Katura T, Sato H, Fuchino Y, Yoshida T, Atsumori H, Kiguchi M, Maki A, Abe M, Tanaka N (2008) Extracting task-related activation components from optical topography measurement using independent components analysis. Journal of biomedical optics 13:054008.

Kirilina E, Jelzow A, Heine A, Niessing M, Wabnitz H, Bruhl R, Ittermann B, Jacobs AM, Tachtsidis I (2012) The physiological origin of task-evoked systemic artefacts in functional near infrared spectroscopy. Neuroimage 61:70-81.

Kleinschmidt A, Muller NG (2010) The blind, the lame, and the poor signals of brain function--a comment on Sirotin and Das (2009). Neuroimage 50:622-625.

Kohno S, Miyai I, Seiyama A, Oda I, Ishikawa A, Tsuneishi S, Amita T, Shimizu K (2007) Removal of the skin blood flow artifact in functional near-infrared spectroscopic imaging data through independent component analysis. J Biomed Optics 12:062111.

Lin Q-H, Liu J, Zheng Y-R, Liang H, Calhoun VD (2010) Semiblind Spatial ICA of fMRI Using Spatial Constraints. Human Brain Mapping 31:1076-1088.

Makeig S, Bell AJ, Jung TP, Sejnowski TJ (1996) Independent component analysis of electroencephalographic data. Advances in Neural Information Processing Systems:145-151.

Marcenko VA, Pastur LA (1967) Distribution of eigenvalues for some sets of random matrices. Mathematics of the USSR-Sbornik 1:457.

McKeown MJ, Sejnowski TJ (1998) Independent component analysis of fMRI data: examining the assumptions. Human Brain Mapping 6:368-372.

Mika S, Ratsch G, Weston J, Scholkopf B, Mullers KR (1999a) Fisher discriminant analysis with kernels. Neural Networks for Signal Processing IX: Proceedings of the 1999 IEEE Signal Processing Society Workshop (Cat No98TH8468).

Mika S, Scholkopf B, Smola AJ, Muller KR, Scholz M, Ratsch G (1999b) Kernel PCA and de-noising in feature spaces. Advances in neural information processing systems 11:536-542.

Minati L, Kress IU, Visani E, Medford N, Critchley HD (2011) Intra- and extra-cranial effects of transient blood pressure changes on brain near-infrared spectroscopy (NIRS) measurements. J Neurosci Methods 197:283-288.

Monasterio V, Clifford GD, Laguna P, Martinez JP (2010) A multilead scheme based on periodic component analysis for T-wave alternans analysis in the ECG. Ann Biomed Eng 38:2532-2541.

Nakada T, Suzuki K, Fujii Y, Matsuzawa H, Kwee IL (2000) Independent component-cross correlation-sequential epoch (ICS) analysis of high field fMRI time series: direct visualization of dual representation of the primary motor cortex in human. Neurosci Res 37:237-244.

Nakamura H, Yoshida M, Kotani M, Akazawa K, Moritani T (2004) The application of independent component analysis to the multi-channel surface electromyographic signals for separation of motor unit action potential trains: part I-measuring techniques. J Electromyogr Kinesiol 14:423-432.

Patel S, Katura T, Maki A, Tachtsidis I (2011) Quantification of Systemic Interference in Optical Topography Data during Frontal Lobe and Motor Cortex Activation: An Independent Component Analysis. Advances in experimental medicine and biology 701:45-51.

Peyrache A, Benchenane K, Khamassi M, Wiener SI, Battaglia FP (2010) Principal component analysis of ensemble recordings reveals cell assemblies at high temporal resolution. J Comput Neurosci 29:309-325.

Plichta MM, Heinzel S, Ehlis AC, Pauli P, Fallgatter AJ (2007) Model-based analysis of rapid event-related functional near-infrared spectroscopy (NIRS) data: a parametric validation study. Neuroimage 35:625-634.

Rao SM, Bandettini PA, Binder JR, Bobholz JA, Hammeke TA, Stein EA, Hyde JS (1996) Relationship between finger movement rate and functional magnetic resonance signal change in human primary motor cortex. Journal of Cerebral Blood Flow and Metabolism 16:1250-1254.

Saager RB, Telleri NL, Berger AJ (2011) Two-detector Corrected Near Infrared Spectroscopy (C-NIRS) detects hemodynamic activation responses more robustly than single-detector NIRS. Neuroimage 55:1679-1685.

Sameni R, Jutten C, Shamsollahi MB (2008) Multichannel electrocardiogram decomposition using periodic component analysis. IEEE Trans Biomed Eng 55:1935-1940.

Sato H, Fuchino Y, Kiguchi M, Katura T, Maki A, Yoro T, Koizumi H (2005) Intersubject variability of near-infrared spectroscopy signals during sensorimotor cortex activation. J Biomed Opt 10:44001.

Sato H, Tanaka N, Uchida M, Hirabayashi Y, Kanai M, Ashida T, Konishi I, Maki A (2006) Wavelet analysis for detecting body-movement artifacts in optical topography signals. Neuroimage 33:580-587.

Saul LK, Allen JB (2001) Periodic component analysis: an eigenvalue method for representing periodic structure in speech. Advances in Neural Information Processing Systems:807-813.

Sirotin YB, Das A (2009) Anticipatory haemodynamic signals in sensory cortex not predicted by local neuronal activity. Nature 457:475-479.

Sirotin YB, Cardoso M, Lima B, Das A (2012) Spatial homogeneity and task-synchrony of the trial-related hemodynamic signal. Neuroimage 59:2783-2797.

Tachtsidis I, Koh PH, Stubbs C, Elwell CE (2010) Functional optical topography analysis using statistical parametric mapping (SPM) methodology with and without physiological confounds. Oxygen Transport to Tissue XXXI:237-243.

Tachtsidis I, Leung TS, Chopra A, Koh PH, Reid CB, Elwell CE (2009) False positives in functional nearinfrared topography. Oxygen Transport to Tissue XXX:307-314.

Takahashi T, Takikawa Y, Kawagoe R, Shibuya S, Iwano T, Kitazawa S (2011) Influence of skin blood flow on near-infrared spectroscopy signals measured on the forehead during a verbal

fluency task. Neuroimage 57:991-1002.

Wigner EP (1955) Characteristic vectors of bordered matrices with infinite dimensions. The Annals of Mathematics 62:548-564.

Wigner EP (1967) Random matrices in physics. SIAM Review 9:1-23.

Wishart J (1928) The generalised product moment distribution in samples from a normal multivariate population. Biometrika 20:32-52.

Worsley KJ, Friston KJ (1995) Analysis of fMRI time-series revisited--again. Neuroimage 2:173-181.

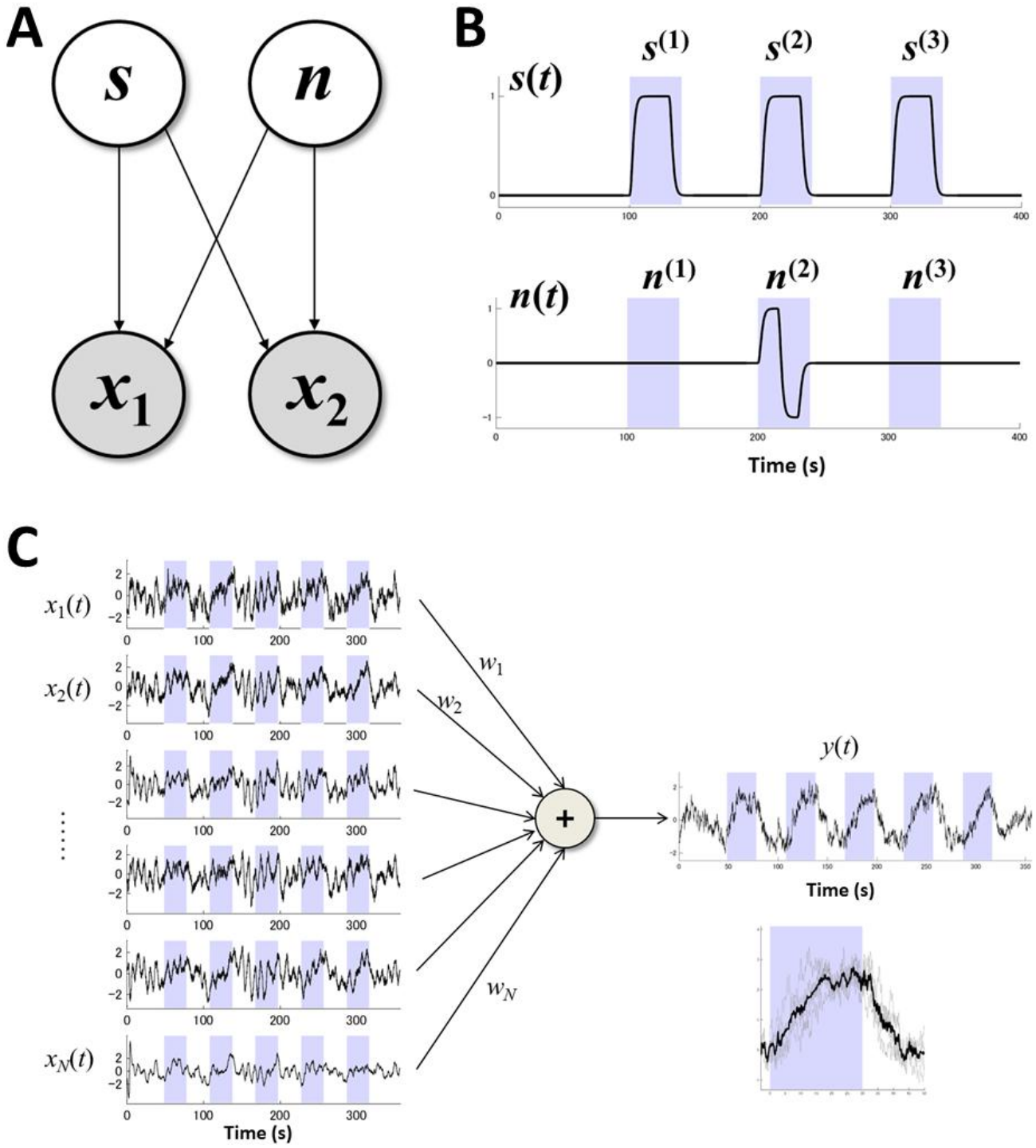
A
s
n
x1
x2
B
s(t)
s(1)
s(2)
s(3)
n(t)
n(1)
n(2)
n(3)
Time (s)
C
x1(t)
x2(t)
xN(t)
w1
w2
wN
+
y(t)
Time (s)
Time (s)

Figure 1

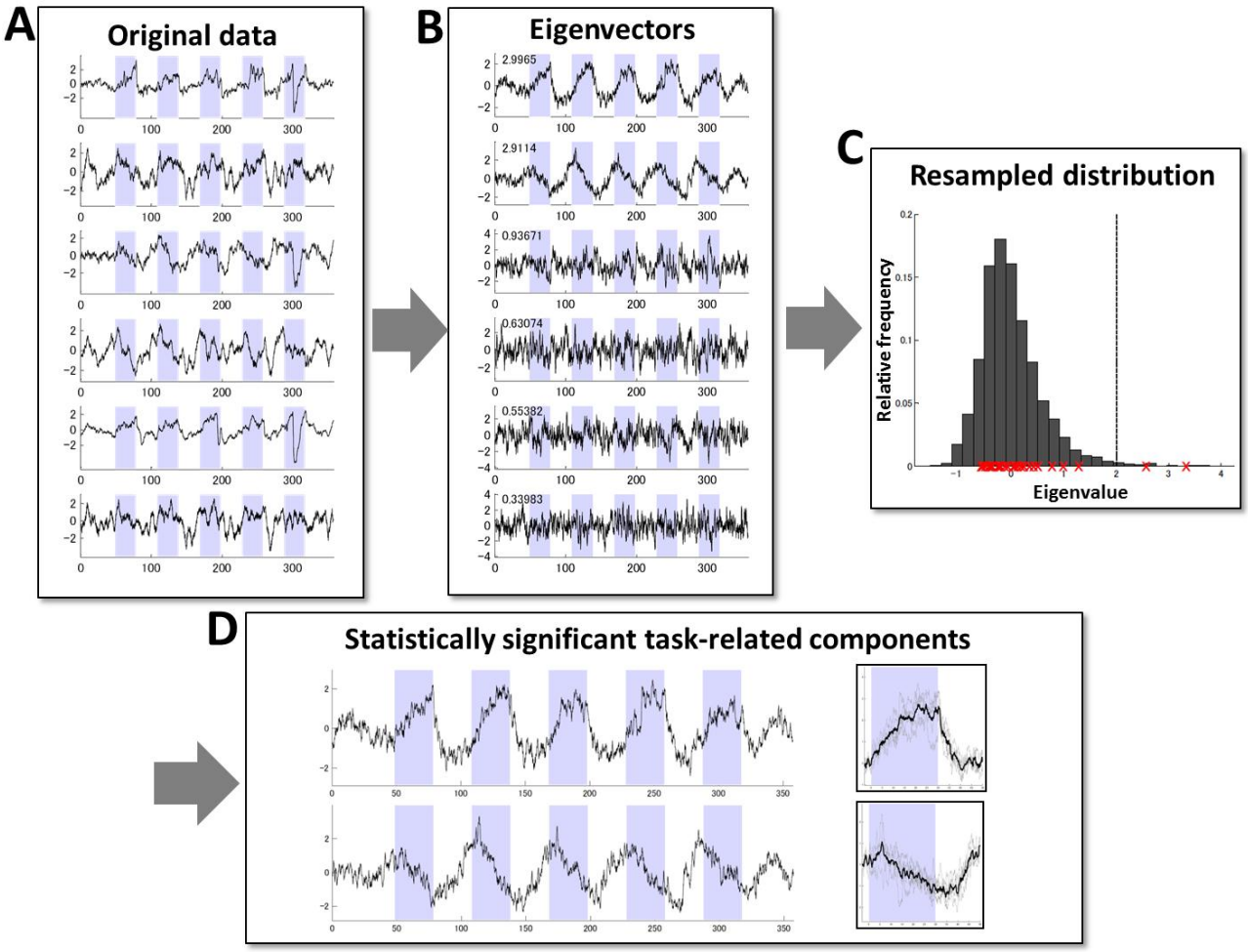
A
Original data
B
Eigenvectors
2.9965
2.9114
0.93671
0.63074
0.55382
0.33983
C
Resampled distribution
Relative frequency
Eigenvalue
D
Statistically significant task-related components

Figure 2

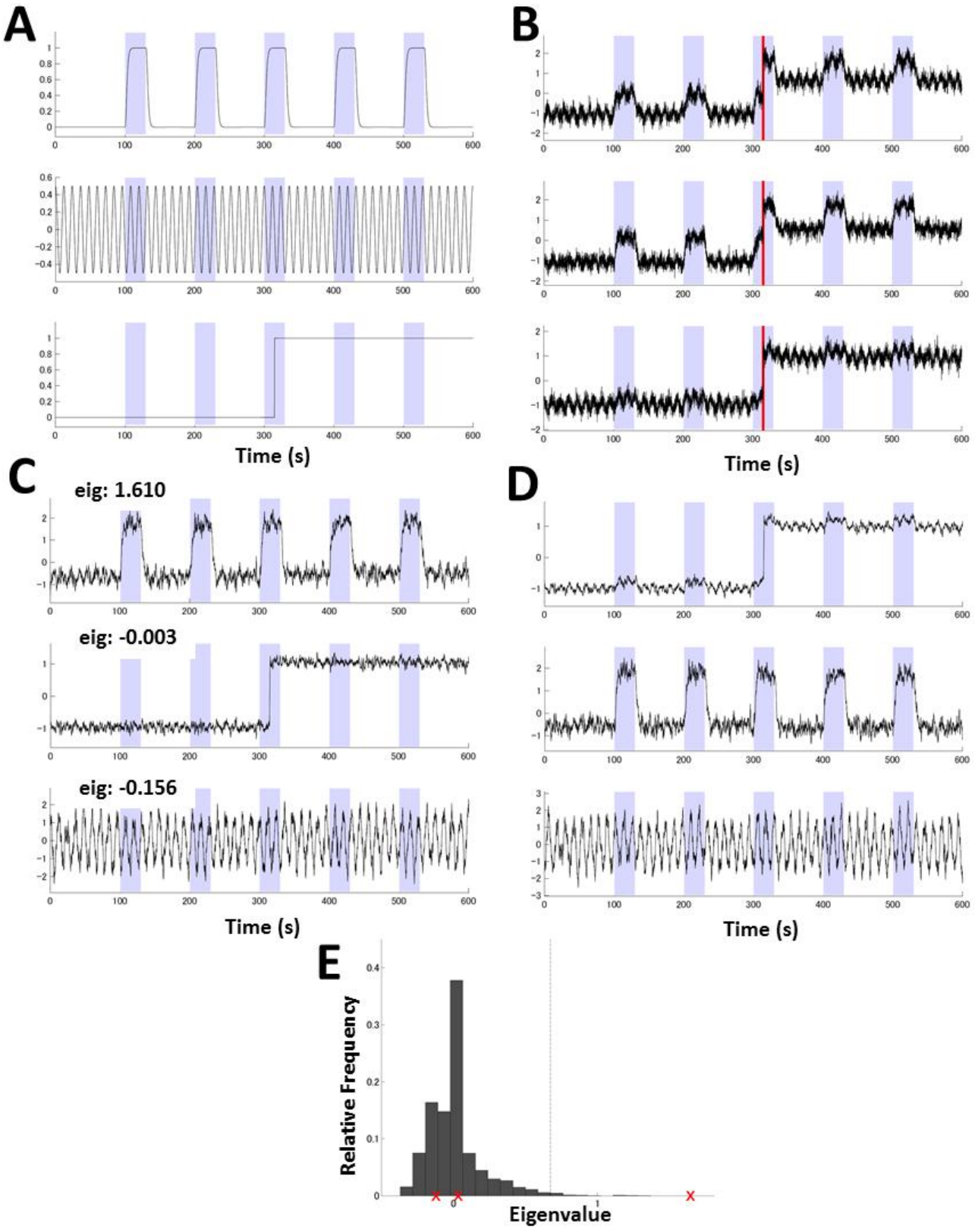
A
B
Time (s)
C
eig: 1.610
eig: -0.003
eig: -0.156
Time (s)
D
Time (s)
E
Relative Frequency
Eigenvalue

Figure 3

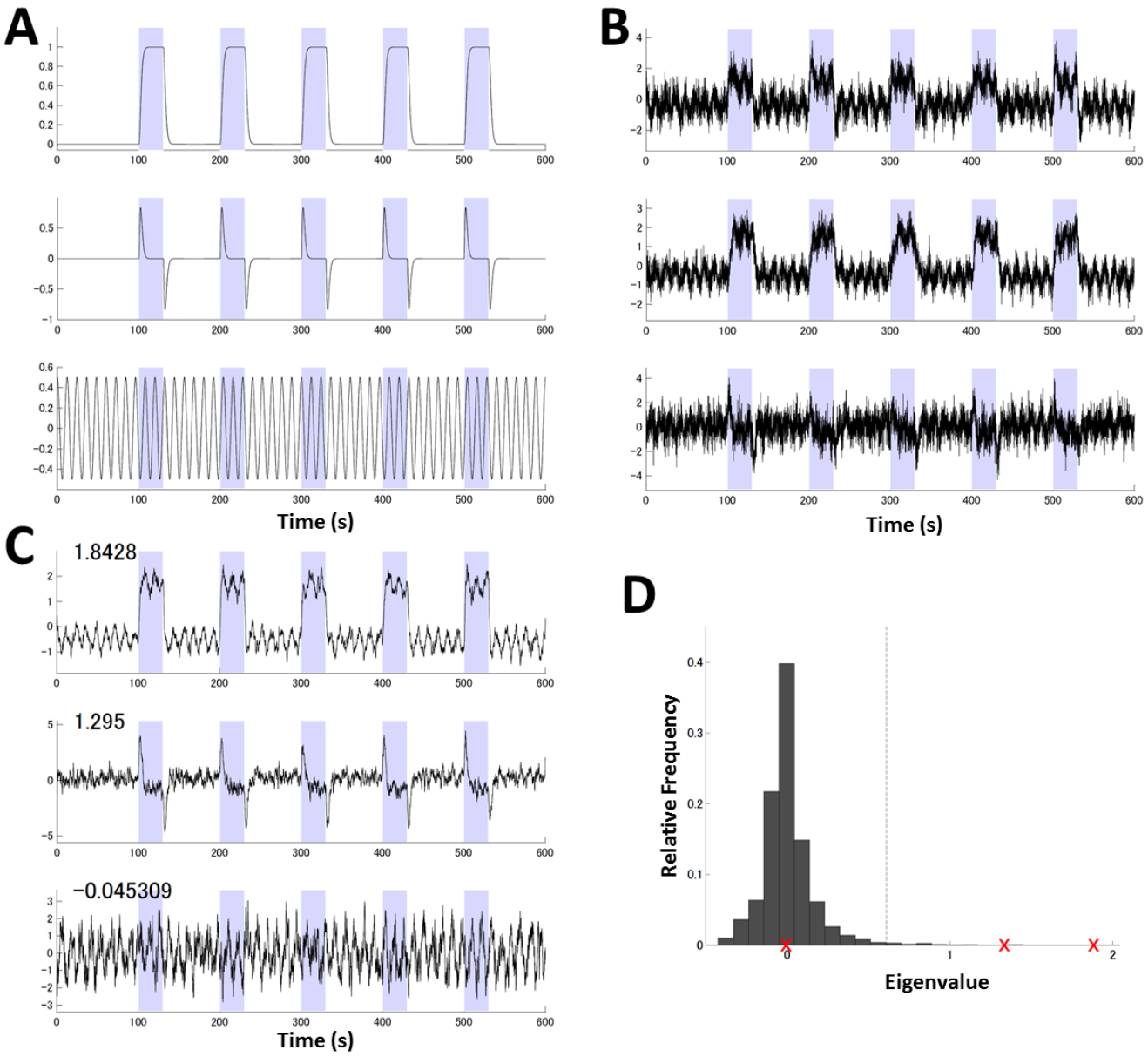
A
B
C
D
Time (s)
Time (s)
1.8428
1.295
−0.045309
Time (s)
Relative Frequency
Eigenvalue

Figure 4

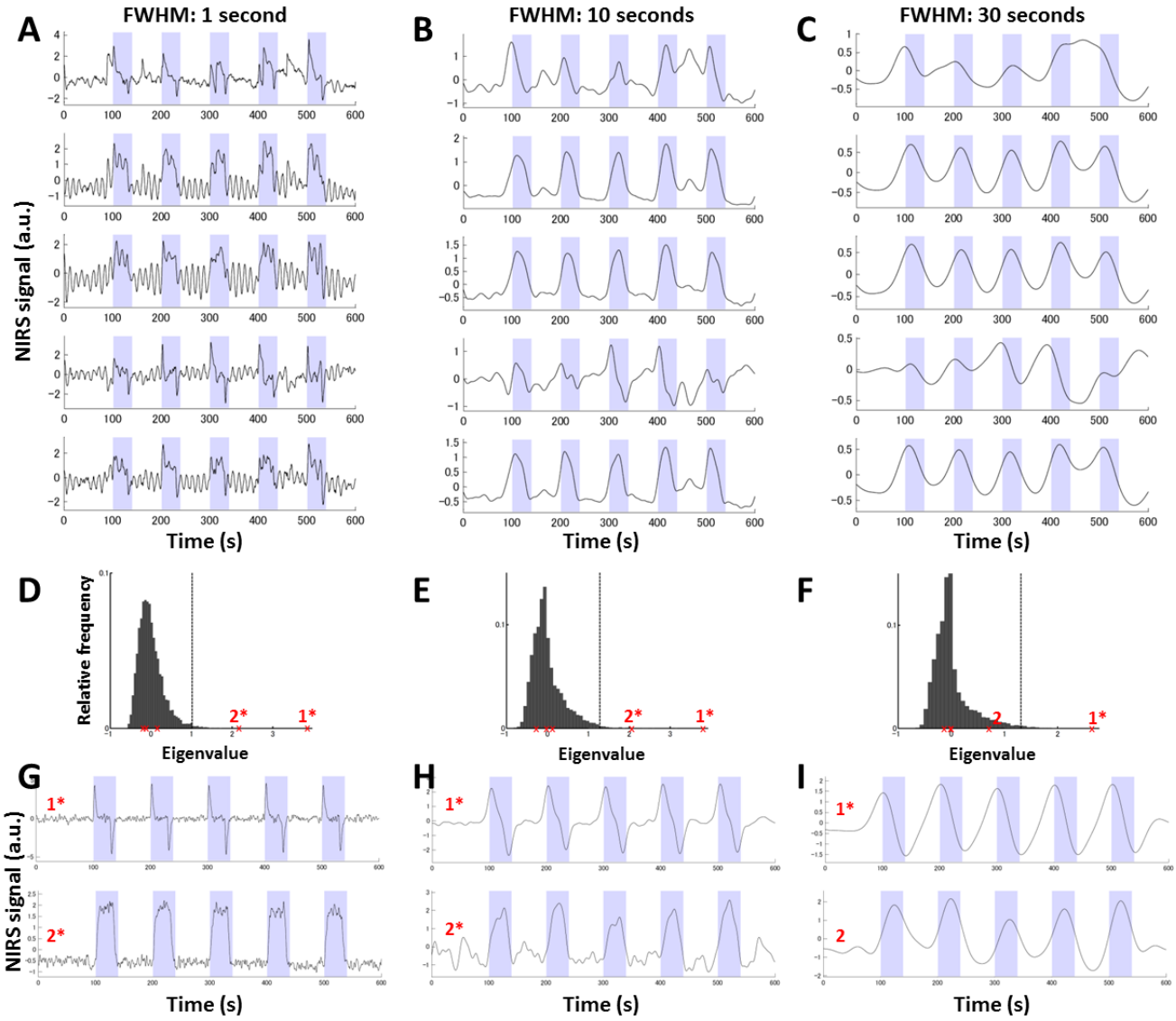
A
FWHM: 1 second
B
FWHM: 10 seconds
C
FWHM: 30 seconds
NIRS signal (a.u.)
Time (s)
D
E
F
Relative frequency
Eigenvalue
1*
2*
2
G
H
I
NIRS signal (a.u.)
Time (s)

Figure 5

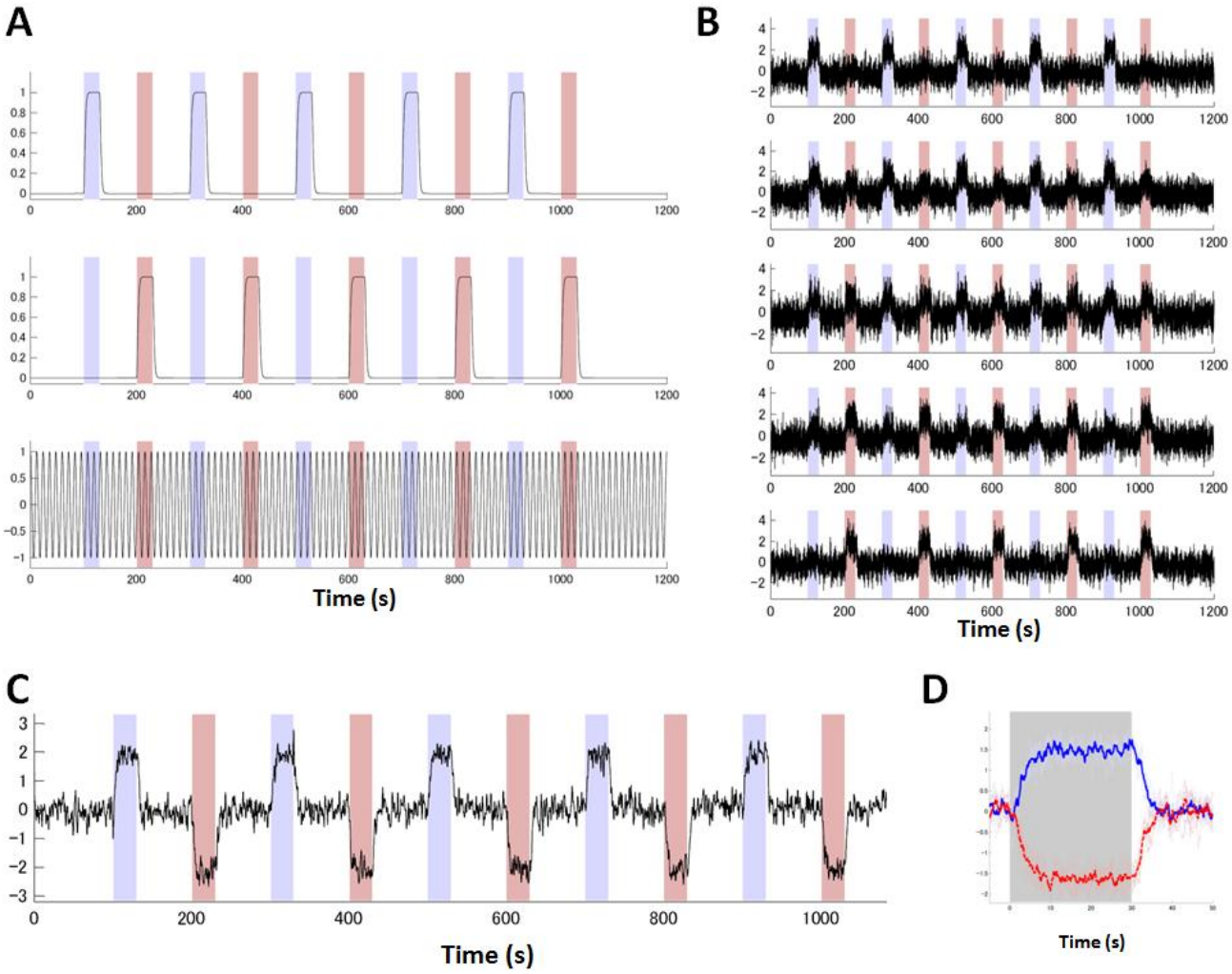

Figure 6

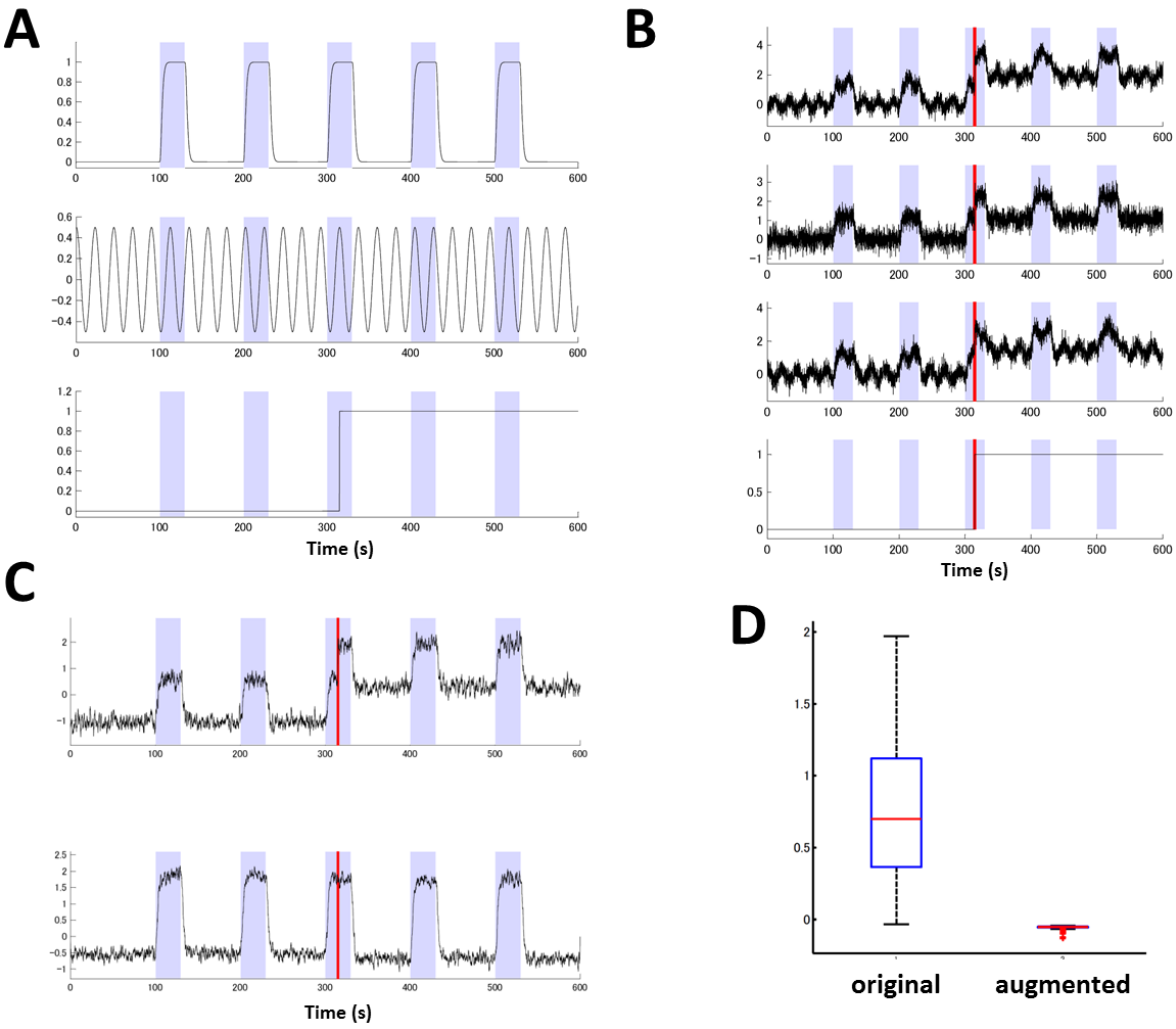

Figure 7

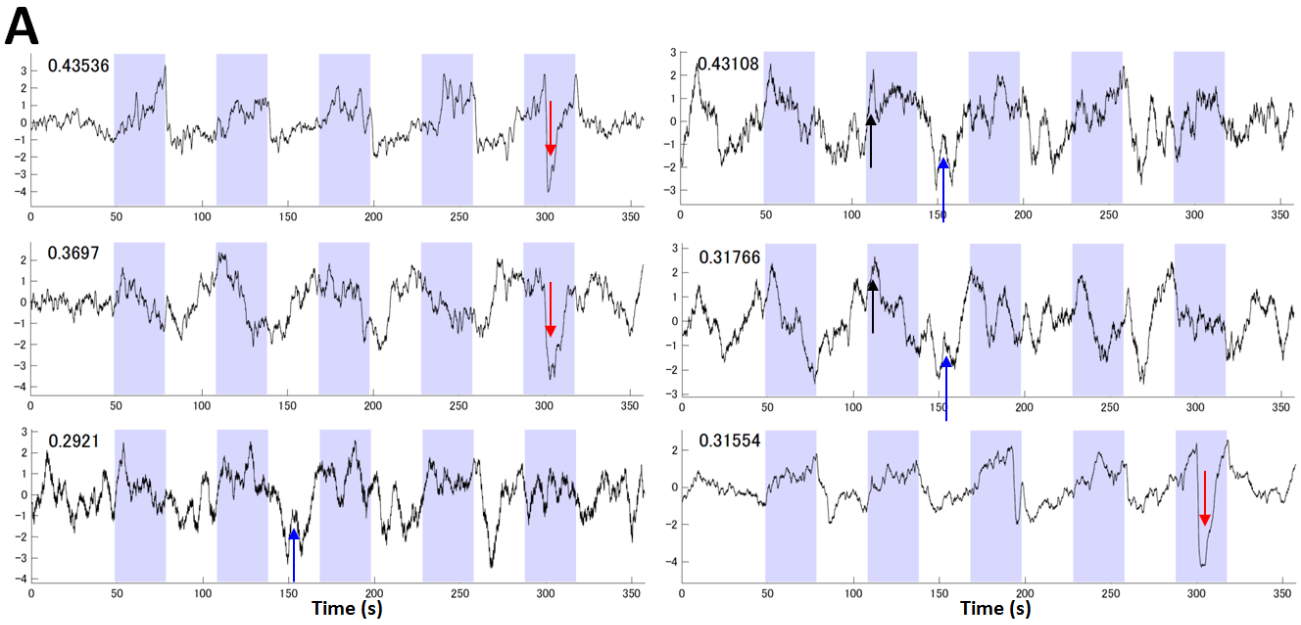
A
0.43536
0.43108
0.3697
0.31766
0.2921
0.31554
Time (s)
Time (s)

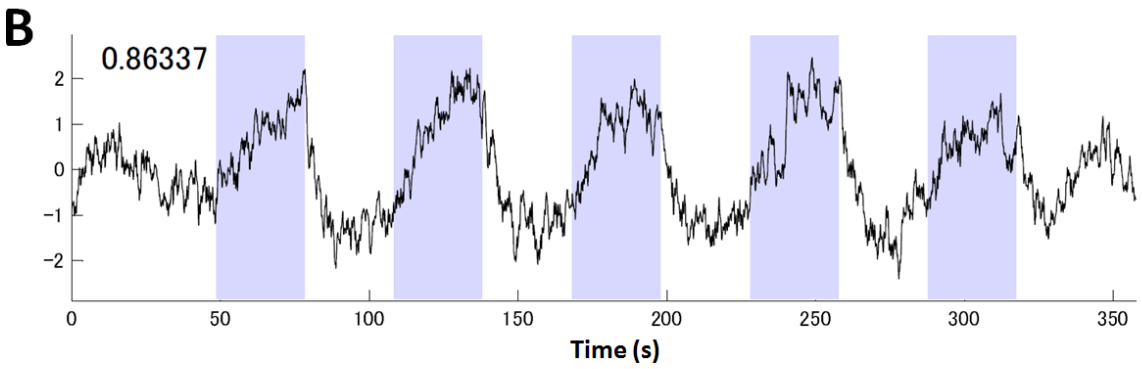
B
0.86337
Time (s)

Figure 8

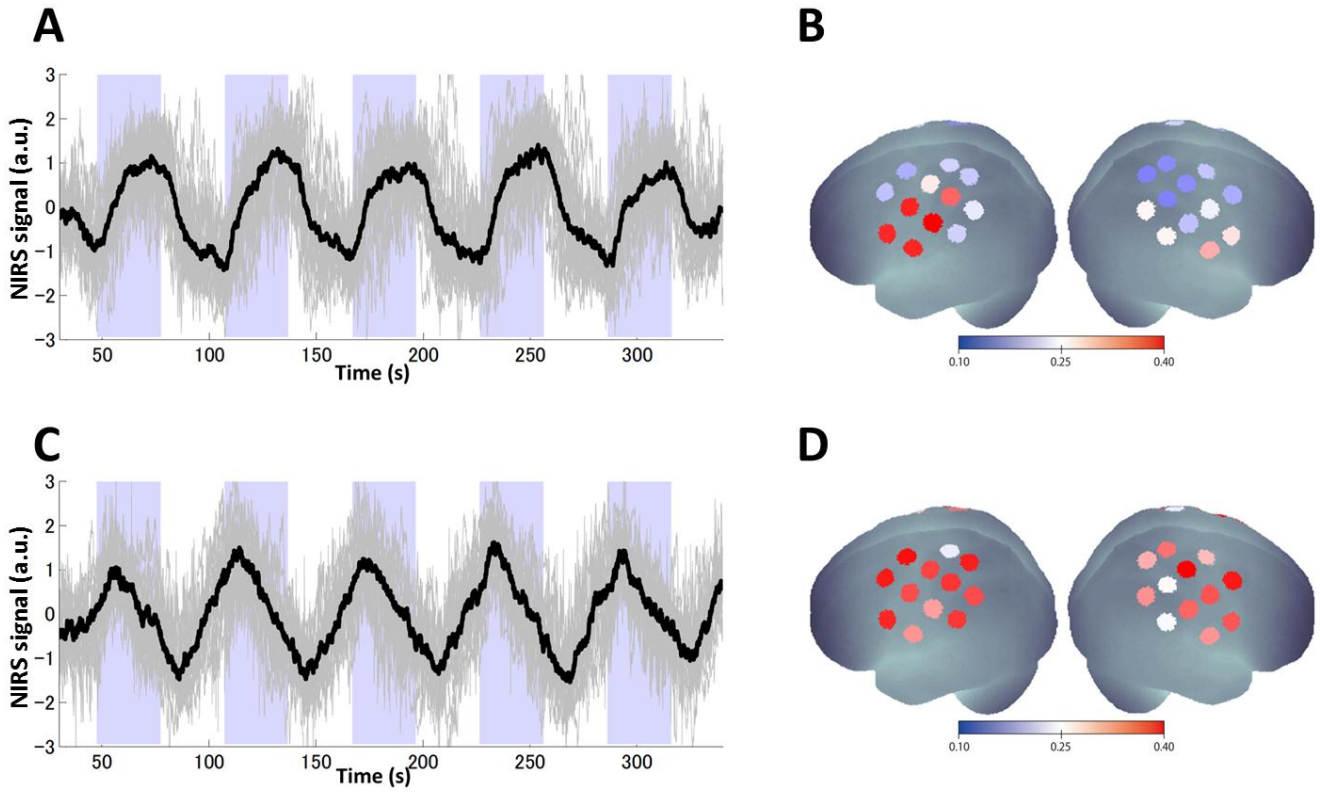
A
B
C
D
NIRS signal (a.u.)
Time (s)
3
2
1
0
−1
−2
−3
50
100
150
200
250
300
0.10
0.25
0.40

Figure 9

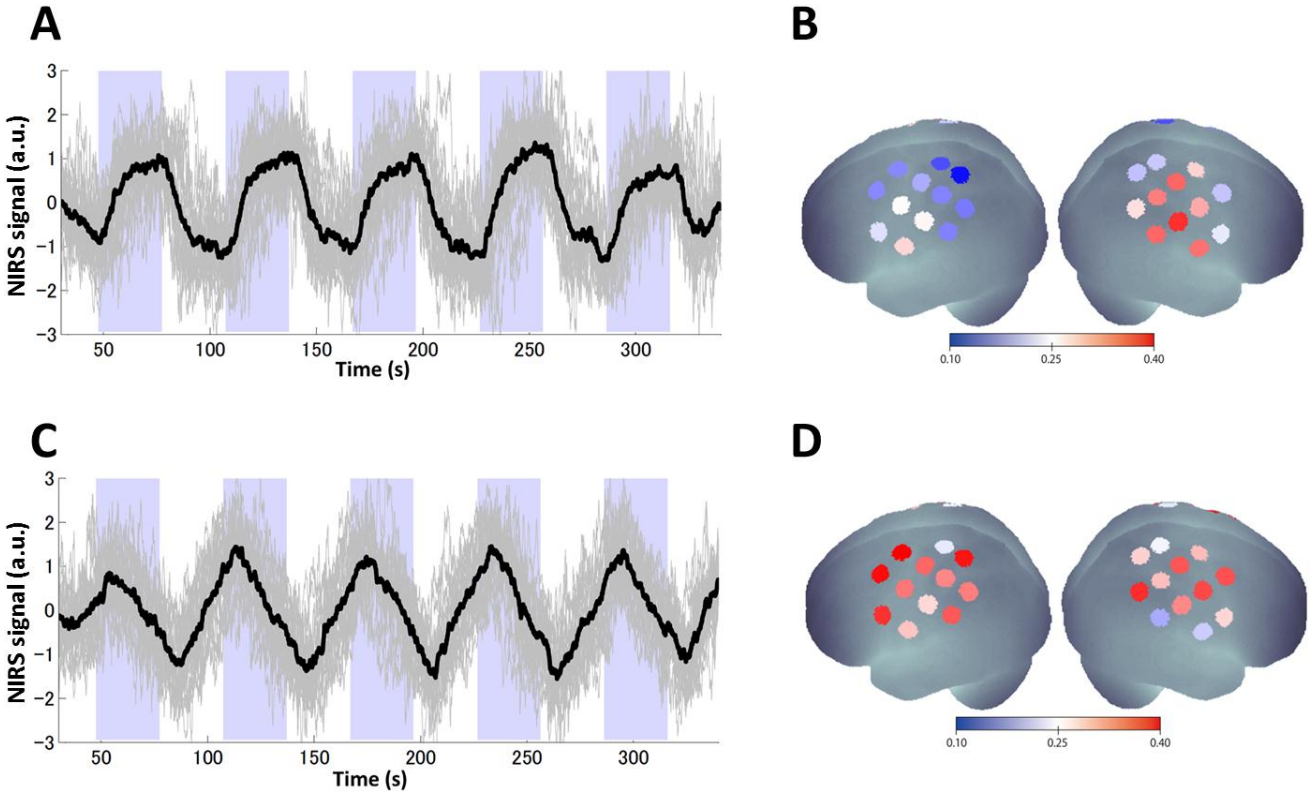
A
B
C
D
NIRS signal (a.u.)
Time (s)
3
2
1
0
−1
−2
−3
50
100
150
200
250
300
0.10
0.25
0.40

Figure 10

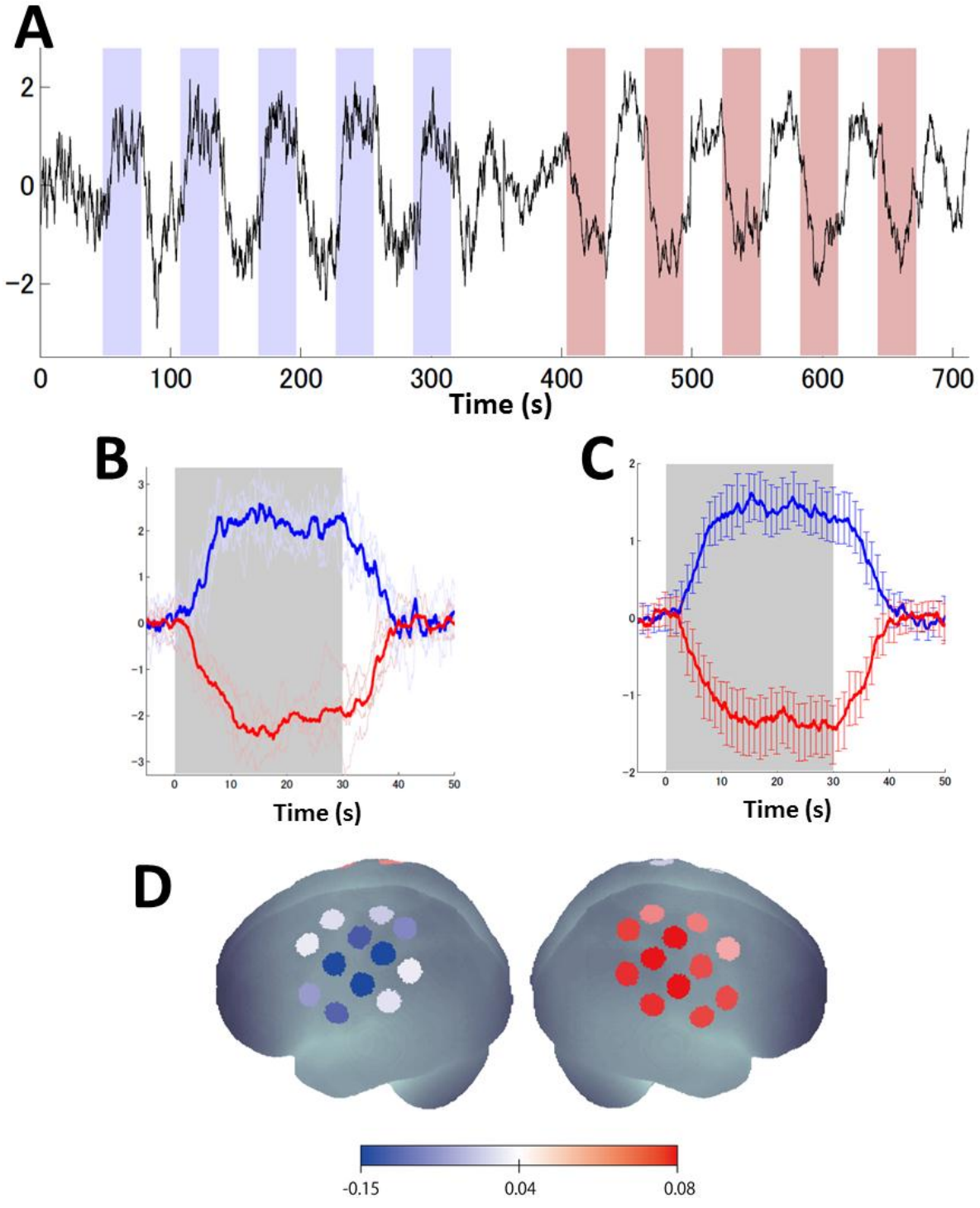
A
2
0
−2
0
100
200
300
400
500
600
700
Time (s)
B
Time (s)
C
Time (s)
D
-0.15
0.04
0.08

Figure 11

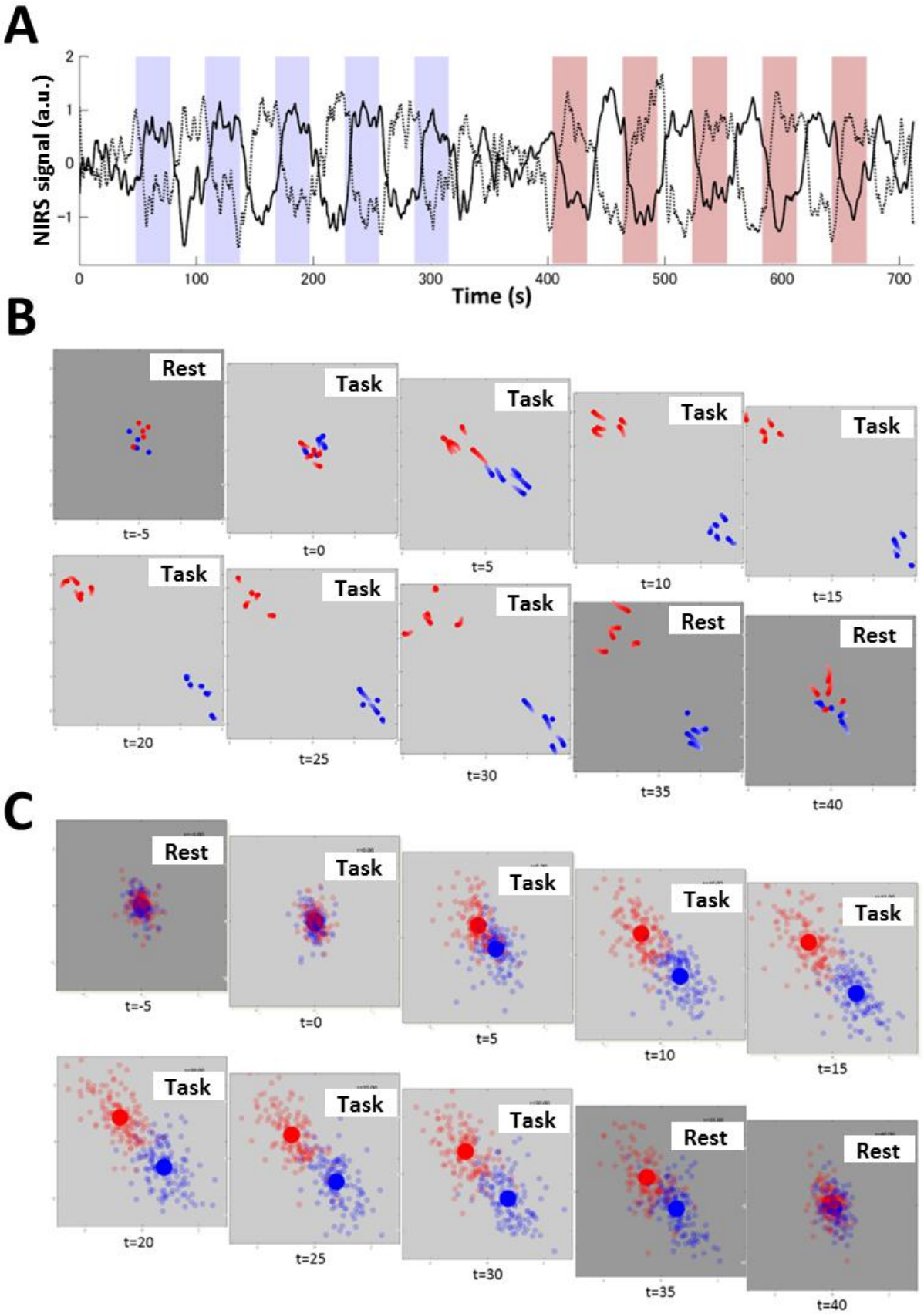
A
NIRS signal (a.u.)
Time (s)
B
Rest
Task
t=-5
t=0
t=5
t=10
t=15
t=20
t=25
t=30
t=35
t=40
C

Figure 12

Supplementary Material

Several additional numerical simulations using synthetic data and analyses to the NIRS data are described for the purpose of testing our proposed method in various conditions.

1. Additional simulations with synthetic data

In the main text TRCA was tested with synthetic data with fixed values of activation amplitudes, activation onsets, and temporal sampling rates. Here we describe additional numerical simulations with synthetic data in which these factors were not held constant but rather variable,

Whereas in the main text systemic and motion artifacts were modeled with simplistic temporal profiles, more realistic forms of systemic and motion artifacts were included here. First, the Mayer wave was a modeled oscillation of 0.083 Hz (12 second period) with 0.011 Hz (90 second period) amplitude modulation as

$$r_2(t) = \cos\left(\frac{2\pi t}{t_1}\right)\left[0.2 + \left|\cos\left(\frac{2\pi t}{t_2}\right)\right|\right] \quad (t_1 = 12 \text{ s},\ t_2 = 90 \text{ s}), \tag{S.1}$$

and non-periodic low-frequency noise was included as

$$r_3(t) : 0.1 \text{ Hz low-pass filtered Gaussian noise } N(0,1). \tag{S.2}$$

A motion artifact was modeled with a sum of decaying exponentials as

$$r_4(t) = \sum_i h_i(t), \text{ where } \quad h_i(t) = \begin{cases} 0 & t < t_i \\ a_i \exp\left(\dfrac{t - t_i}{\tau_i}\right) & t \geq t_i \end{cases} \tag{S.3}$$

The amplitudes (a_i) and the time constants (τ_i) were random variables, sampled from $U(1, 2)$ and $U(10, 30)$, respectively. Here, $U(a, b)$ denotes a uniform distribution ranging from a to b. Onset intervals between t_i and t_{i+1} were randomly sampled from $U(20, 120)$.

For the simulations of Sections 1.1 and 1.2, the mixing matrix was

$$\mathbf{A} = \begin{pmatrix} 1 & 1 & 1 & 2 \\ 1 & 1 & 1 & 2 \\ 1 & 1 & 1 & 2 \\ 1 & 1 & 1 & 2 \end{pmatrix} + \begin{pmatrix} \eta_{11} & \eta_{12} & \eta_{13} & \eta_{14} \\ \eta_{21} & \eta_{22} & \eta_{23} & \eta_{24} \\ \eta_{31} & \eta_{32} & \eta_{33} & \eta_{34} \\ \eta_{41} & \eta_{42} & \eta_{43} & \eta_{44} \end{pmatrix}, \tag{S.4}$$

where $\eta \sim N\left(0, 0.5^2\right)$, and for the simulation of Section 1.3,

$$\mathbf{A} = \begin{pmatrix} 1 & 1 & 0.5 & 0.5 & 0.5 \\ 1 & 1 & 0.5 & 0.5 & 0.5 \\ 1 & 1 & 0.5 & 0.5 & 0.5 \\ 1 & 1 & 0.5 & 0.5 & 0.5 \\ 1 & 1 & 0.5 & 0.5 & 0.5 \end{pmatrix} + \begin{pmatrix} \eta_{11} & \eta_{12} & \eta_{13} & \eta_{14} & \eta_{15} \\ \eta_{21} & \eta_{22} & \eta_{23} & \eta_{24} & \eta_{25} \\ \eta_{31} & \eta_{32} & \eta_{33} & \eta_{34} & \eta_{35} \\ \eta_{41} & \eta_{42} & \eta_{43} & \eta_{44} & \eta_{45} \\ \eta_{51} & \eta_{52} & \eta_{53} & \eta_{54} & \eta_{55} \end{pmatrix} \tag{S.5}$$

where $\eta \sim N\left(0, 0.5^2\right)$.

1.1. Variable activation amplitudes

First we examined when amplitudes of task-related hemodynamic responses were not fixed but rather variable block by block. Our task-related component $r_1(t)$ was created as described in the main text except that the amplitude was not fixed at one but was sampled from *U*(1, 3) in every task block (Suppl. Fig. 1A). When TRCA was applied to observed signals (Suppl. Fig. 1B), the simulated hemodynamic response with variable activation amplitudes was recovered as the dominant TRC (Suppl. Figs. 1C and 1D).

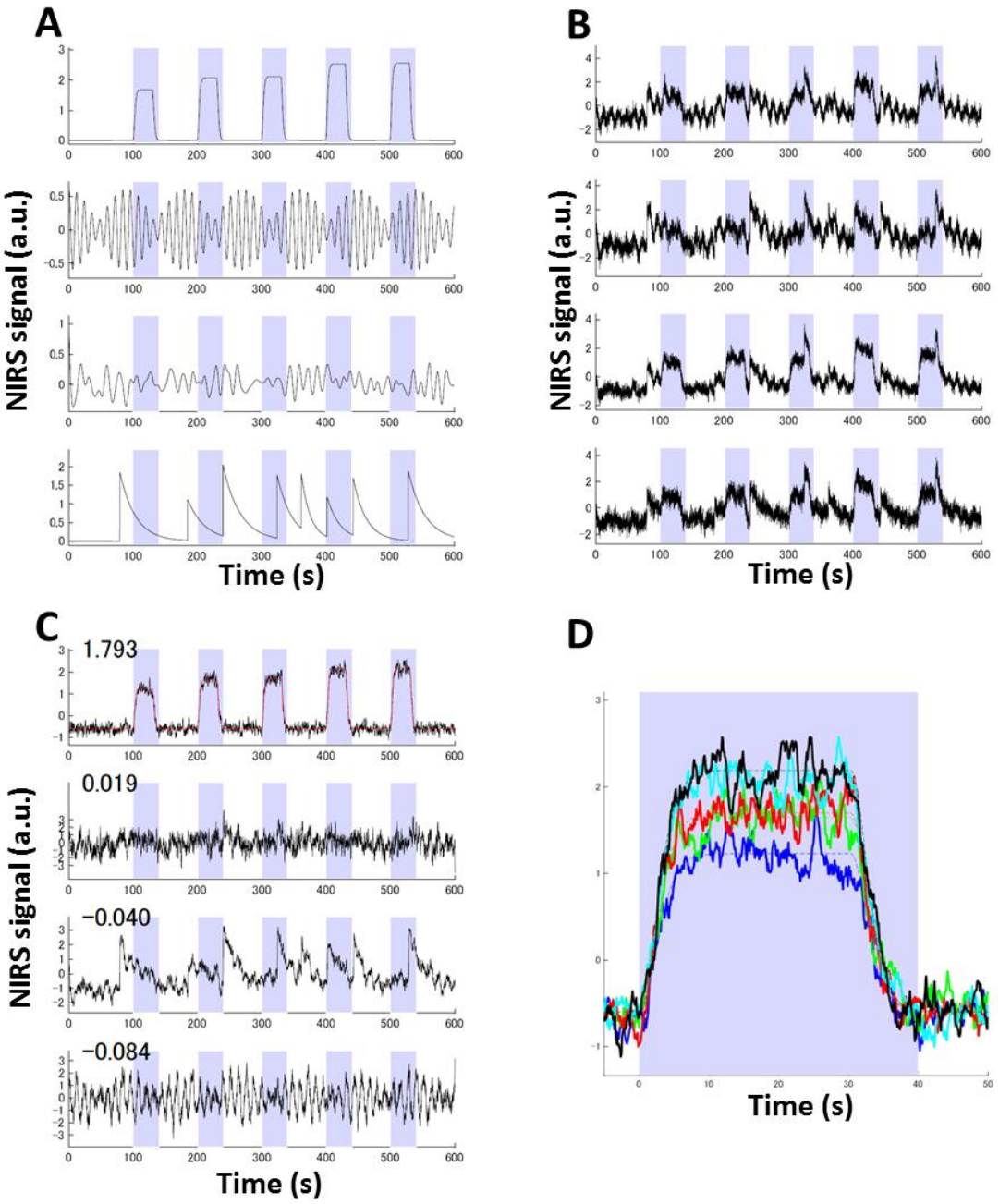

Supplementary Figure 1. Extraction of task-related component with variable activation amplitudes. Original signals in (A) (from top to bottom: task-related hemodynamics, Mayer wave, low-pass filtered Gaussian noise, and motion artifacts) were randomly mixed to give observed time courses in (B). Extracted task-related components are shown with corresponding eigenvalules in (C). The dominat TRC (thick colored lines) was block-by-block compared with $r_1(t)$ (thin, dashed colored lines).

1.2. Variable activation onsets

We then tested the case when activation onsets were not constant but rather changed from 0 to 8

in steps of 2 seconds (Suppl. Fig 2A). The duration of activation was held constant.). In this case, there were a few seconds that the task-related hemodynamic responses did not overlap, so this simulation provided a non-trivial test of our method. Our numerical simulation demonstrates that TRCA was robust against a sight difference in activation onsets (Suppl. Figs. C and D). The simulation result indicates that TRCA is able to extract task-related components even when activation amplitudes or onsets are not constant.

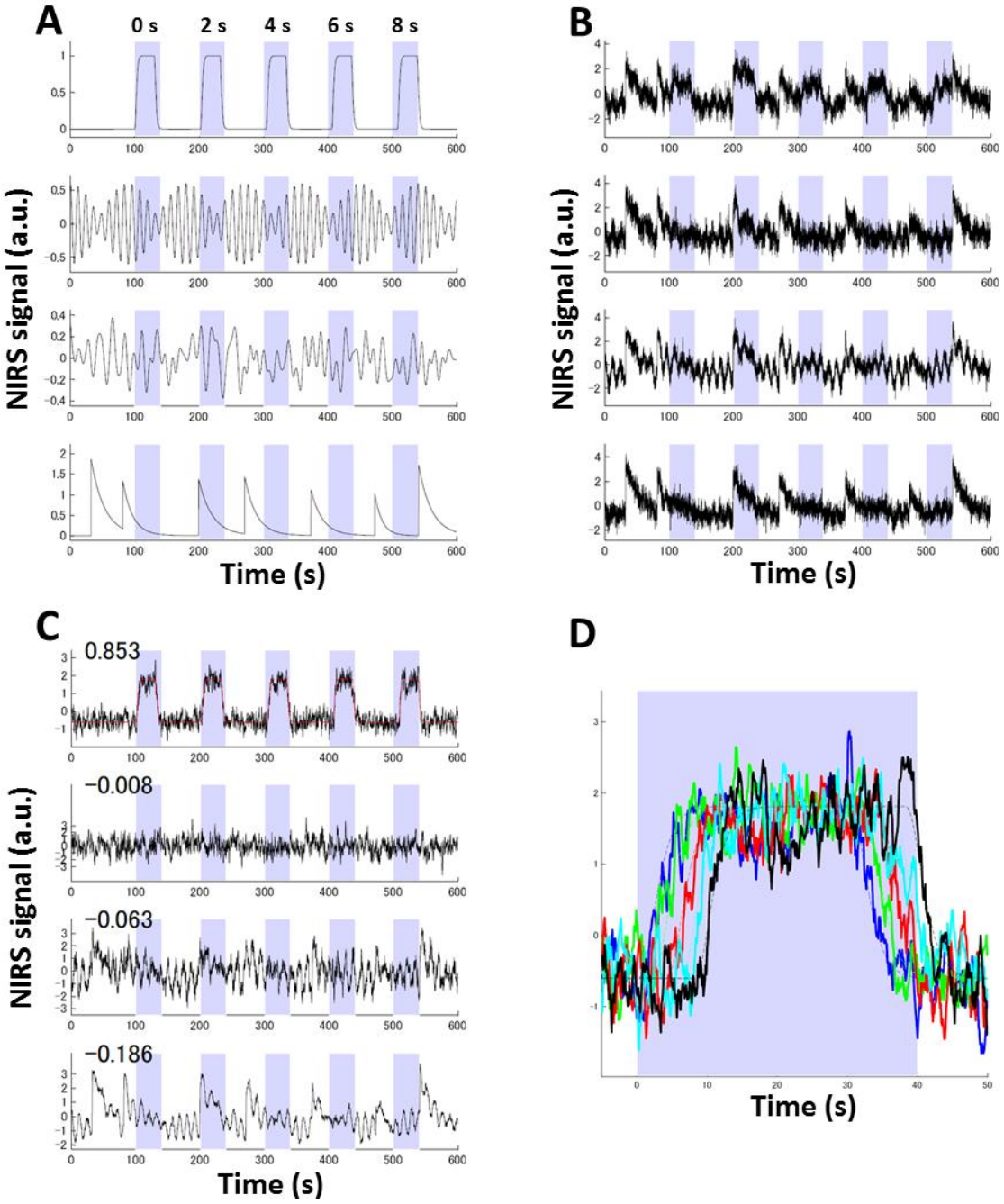

Supplementary Figure 2. Extraction of task-related component with variable activation onsets. (A) Original signals and (B) synthetic observed time courses. (C) Extracted task-related components with corresponding eigenvalules and (D) block-by-block comparison between the dominat TRC (thick colored lines) and $r_1(t)$ (thin, dashed colored lines).

1.3. Sampling rates

In the main text the temporal sampling rate was fixed at 10 Hz, and here a simulation was performed to see whether and how temporal sampling affected the statistical significance. The synthetic data with two task-related components (one with sustained activations and another with transient activations) and three artifact components were created with the sampling rate of 10 Hz. TRCA was applied to this 10-Hz data as well as down-sampled data (2 Hz and 0.5 Hz). The two task-related components were statistically identified and three systemic and motion artifacts were statistically rejected even with the 20-fold down-sampled data, though the wave forms were degraded considerably (Suppl. Fig. 3). With this simulation result, we conclude that our method is capable of robustly detecting task-related components for a wide range of sampling rates.

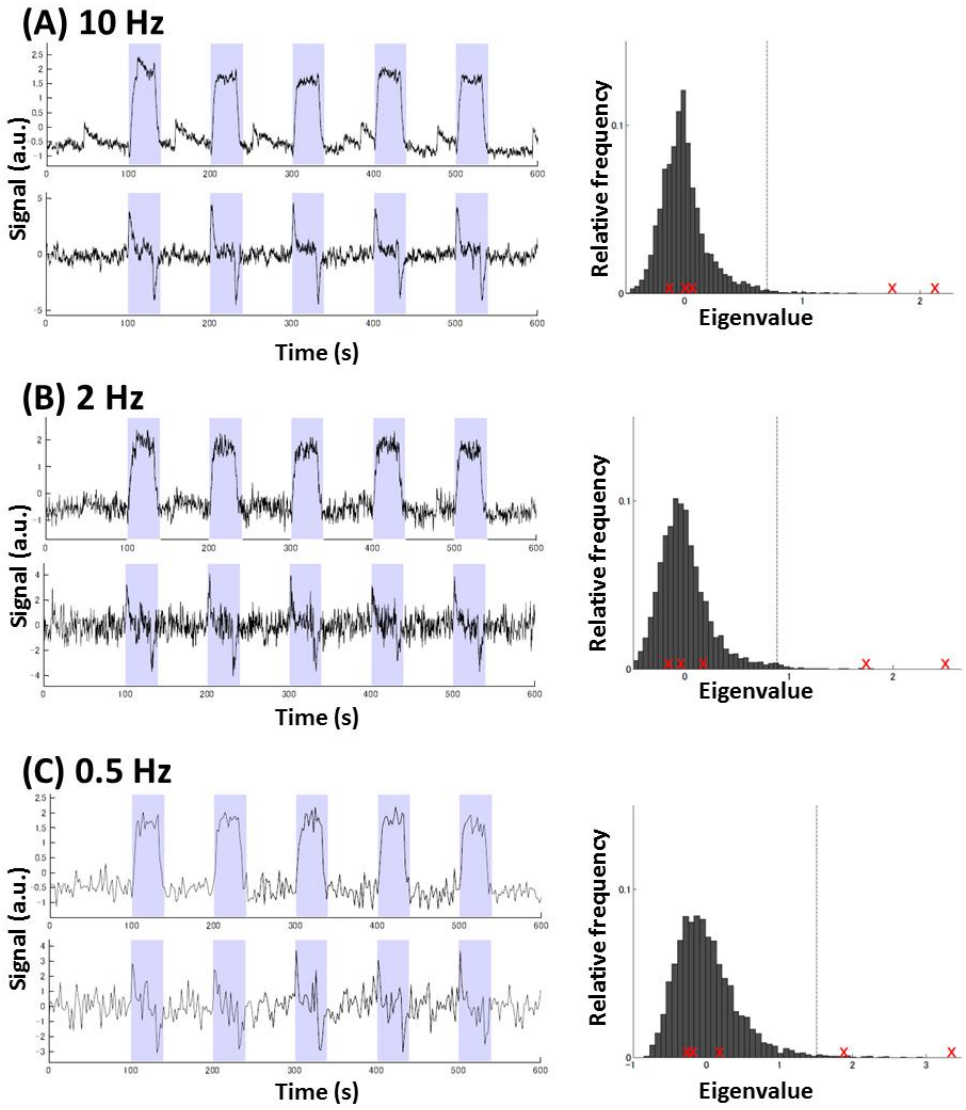

Supplementary Figure 3. Effect of temporal sampling rates on statistical test. Two dominant task-related components and results of resampling statistical test for temporal sampling rate of (A) 10 Hz, (B) 2 Hz and (C) 0.5 Hz.

2. Event-related experiment

In the main text our method was applied to block-design experiments, and here we show that our method is also applicable to event-related experiments. To create a simulated hemodynamic response in an event-related design experiment, task onset timings (t_i) were created in a way that two successive timings were sampled from $U(1, 50)$. Then, a box-car function of three seconds and unit height was added for every event onset. A hemodynamic time course was modeled as a convolution between box-car function and hemodynamic response function (see the top in Suppl. Fig. 4A). Note that some closely located events produced overlapped hemodynamic responses. TRCA was applied to randomly mixed data (Suppl. Fig. 4B), and the task period included five seconds before and ten seconds after each event onset. The results shown in Suppl. Figs. 4C and 4D demonstrate that TRCA was able to extract task-related responses in an event-related experiment.

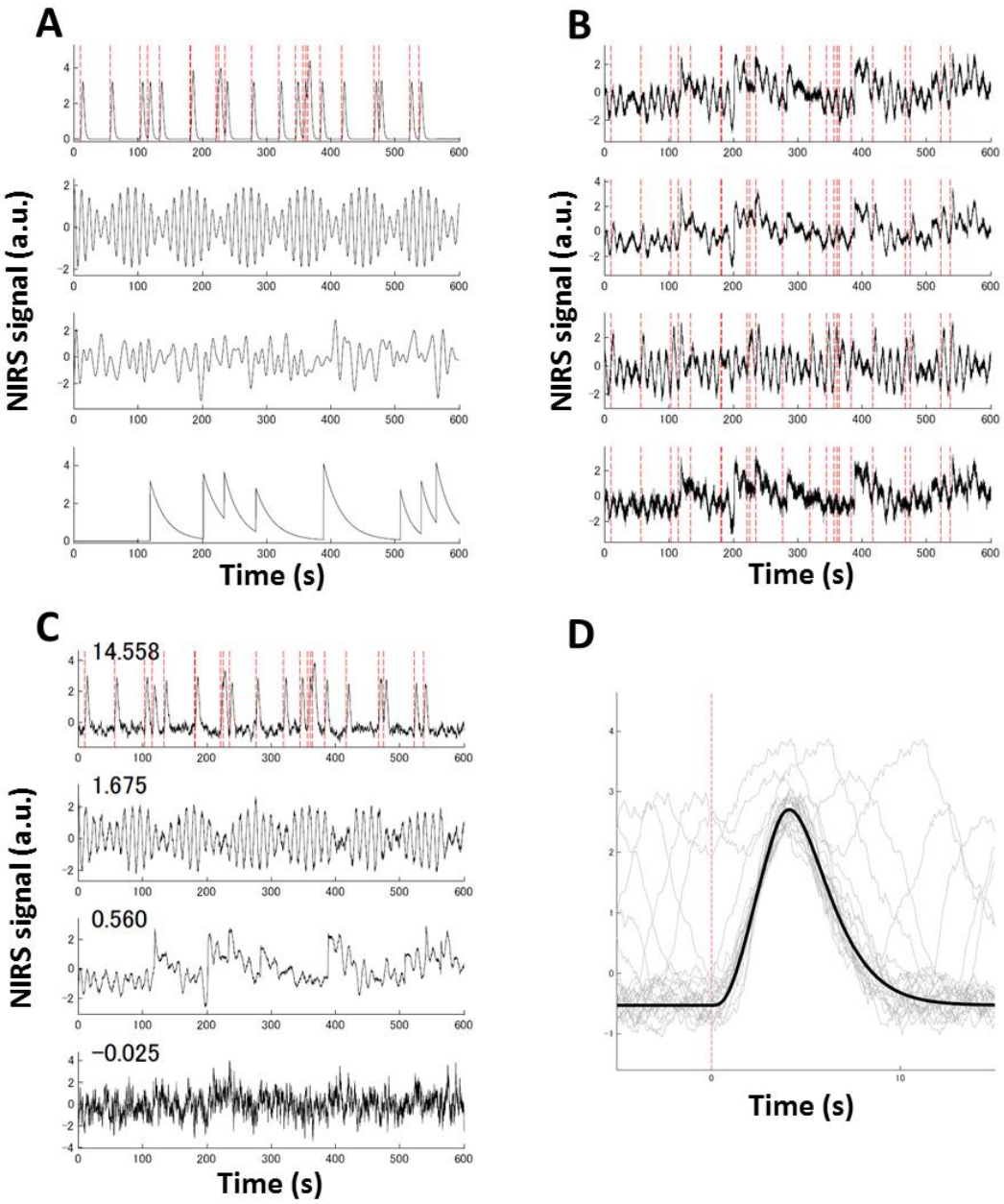

Supplementary Figure 4. Application of TRCA to an event-related experiment. (A) Original signals, (B) input time courses, and (C) Extracted task-related components with corresponding eigenvalules. Vertical red dashed lines denote the timings of event onsets. (D) Dominant TRC aligned with event onsets (gray lines). The black thick line denotes the actual hemodynamic response used to create the synthetic data (i.e., five-second box-car function convolved with hemodynamic response function).

3. Additional analysis with NIRS data

3.1. Number of task blocks

Throughout the paper, data with five blocks were analyzed and here how the number of blocks affected our analysis results. Particularly we wanted to examine any practice or habituation effects in the course of experiment, so we applied TRCA to the initial or the final three blocks of the finger-tapping data. Dominant TRCs derived from the initial (red) or the final (blue) three blocks were similar to those derived from the five blocks (black). Therefore, with this dataset, the number of blocks had little effect on the extracted TRCs, and almost no learning or habituation effect was observed. This was probably because the task was simple finger tapping that required little or no prior training.

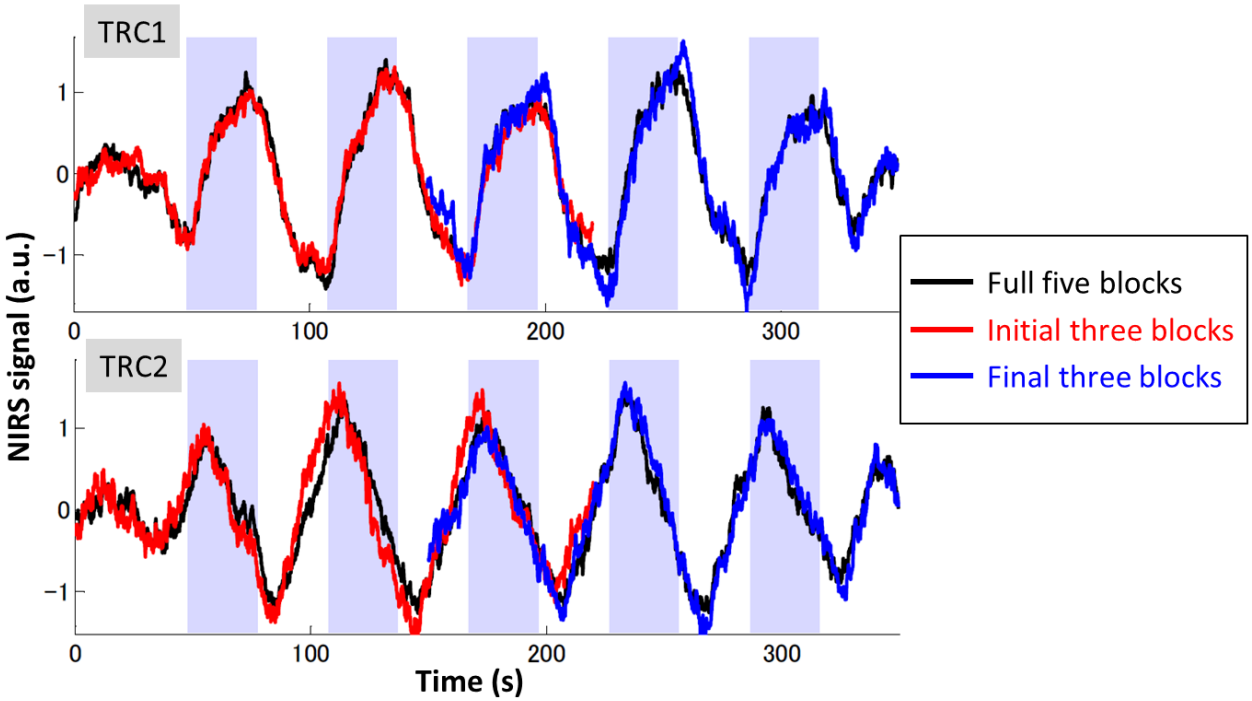

Supplementary Figure 5. Effect of block number. Dominant TRCs computed from the initial three (red) or the final three (blue) blocks (shown only for the right finger-tapping data and similar results obtained for the left finger-tapping data.). The TRCs computed from the five blocks (black) is included for comparison.

3.2. Number of channels

Next we investigated the effect of reduced number of NIRS channels on our analysis. We applied our method to the NIRS data with two sets of reduced NIRS channels (12 out of the full 24 channels). Although slightly noisy, TRCs computed from the reduced sets of NIRS channels closely matched with those computed from the full set. Therefore, for this finger-tapping data, our method was found to be robust even when the channel number was halved.

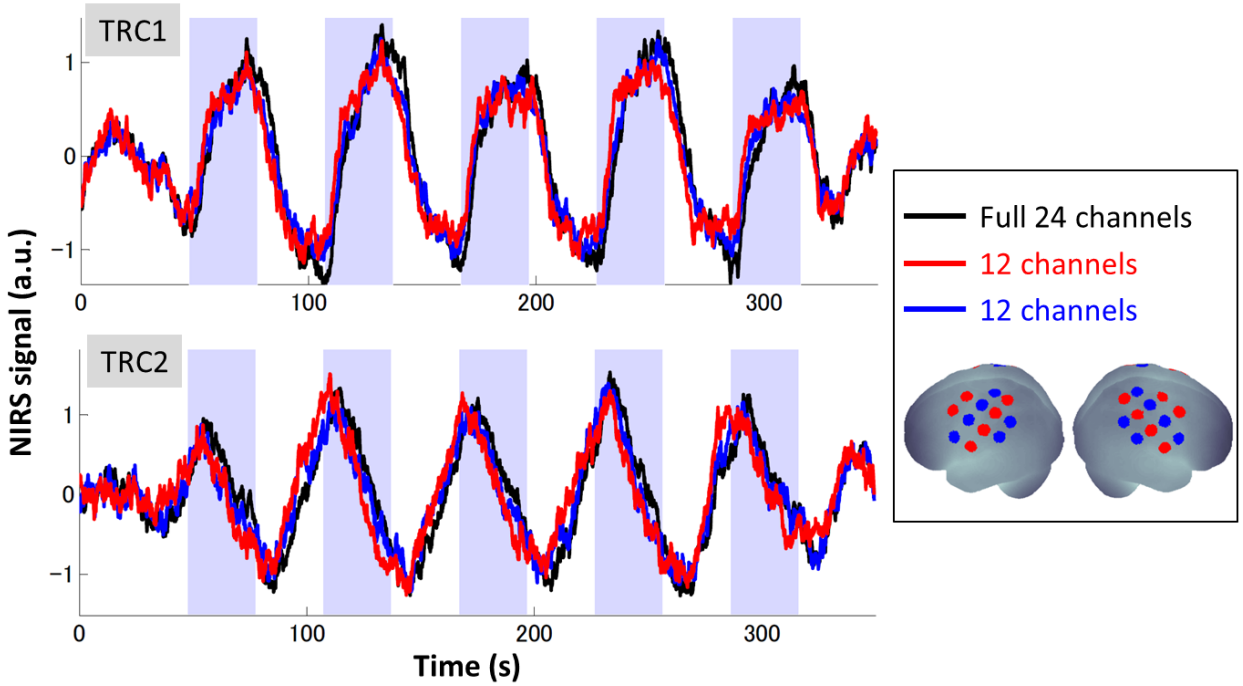

Supplementary Figure 6. Effect of channel number. Dominant TRCs are computed from two reduced sets of channels (corresponding channel sets shown with the same colors in the inset). The TRCs computed from the full number of channels (black) is included for comparison. Shown only for the right finger-tapping data and similar results obtained for the left finger-tapping data.

4. Raw NIRS signals that highly correlated with piece-wise linear component

There were two dominant task-related components; a gradually changing time course, and

another piece-wise linear component. We noticed that the piece-wise component matched closely to a temporal derivative of the gradually changing component (Suppl. Fig. 7A), and that some raw time courses were highly similar to the piece-wise linear component (Suppl. Figs. 7B & 7C).

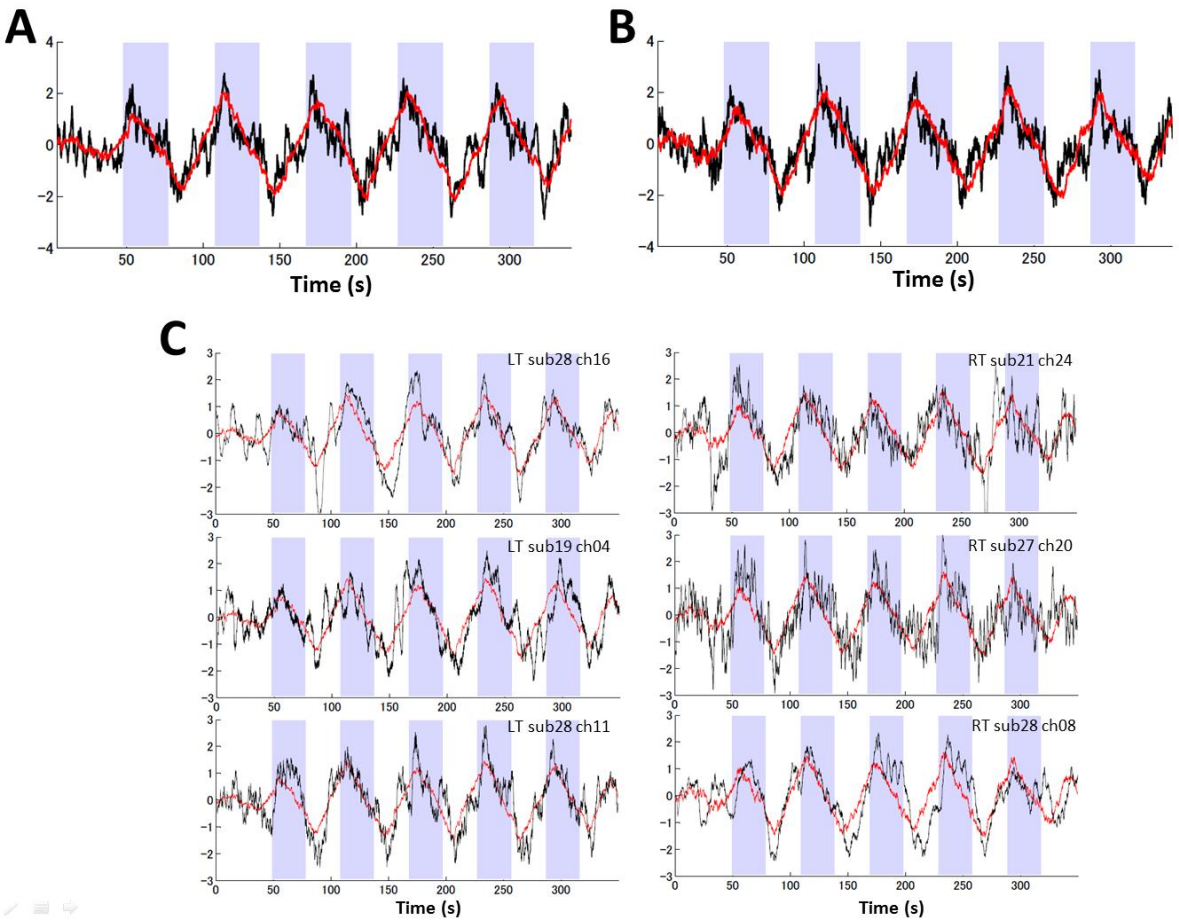

Supplementary Figure 7. Piece-wise linear component compared with the temporal derivative of hemodynamic response component (black) for (A) left- and (B) right-finger tapping. (C) Raw time courses that resembled the piece-wise linear component. Each time course is labeled with task type (LT: left tapping, RT: right tapping), subject number, and channel number.